

Single-qubit operations in the double-donor structure
driven by optical and voltage pulses

Alexander V. Tsukanov

Institute of Physics and Technology, Russian Academy of Sciences

Nakhimovsky pr. 34, Moscow 117218, Russia

E-mail: tsukanov@ftian.oivta.ru

Abstract

We study theoretically the quantum dynamics of an electron in the singly-ionized double-donor structure in the semiconductor host under the influence of laser pulses whose frequencies are close to structure resonant frequencies. This system can be used as a charge qubit where the logical states are defined by the lowest two energy states of the remaining valence electron localized around one or another donor. The quantum operations are performed via resonant or Raman-like transitions between the localized (qubit) states and the excited states delocalized over the structure, combined with phase shifts between qubit states generated by voltage pulses. The possibility of realization of arbitrary single-qubit rotations is demonstrated.

PACS number(s): 03.67.Lx, 78.67.-n, 85.35.-p

I. INTRODUCTION

In view of recent progress in the development of the controlled-donor implantation techniques [1], Kane's paradigm of the solid-state quantum computations [2] has gained new insights. The alternative schemes using the orbital [3, 4] or spin [5, 6] degrees of freedom of the donor-bounded electrons to encode the quantum information instead of the nuclear donor spins, have been proposed. Besides, several refinements of the original proposal concerning the initialization [7] and read-out [8, 9, 10, 11] as well as the information transfer through the quantum networks [12, 13, 14] have been made.

In particular, the pair of donors sharing an electron has been considered as very promising candidate for the solid-state qubit embodiment [3]. The qubit is presented by the electron orbital states positioned at the different donors. There are two main driving mechanisms for the coherent electron evolution defining a quantum operation on such a qubit. First uses the electric fields through an application of the adiabatically switched voltages to the surface gates placed above the donor structure to modify the confinement potential, thus varying the electron tunneling rates between neighboring donors [3, 15, 16]. The desired state of the qubit is realized by an appropriate choice of the voltage parameters. The second scheme relies upon the optical dipole transitions between the size-quantized one-electron levels induced by the resonant pulses [17, 18]. This technique requires one to irradiate the donors encapsulated into near-surface semiconductor layers by laser pulses with

frequencies lying in terahertz range. Such kind of radiation sources is currently under extensive exploration. To all appearances, the quantum cascade lasers [19] in which photon generation takes place via electronic intersubband transitions in semiconductor heterostructures, will be able in near future to cover this frequency range. As it was shown, an arbitrary single-qubit operation can be achieved with two simultaneously switched pulses connecting the qubit states via the excitation of the state delocalized over the structure. The latter scheme is likely to be more preferable than the former due to its higher selectivity and lower field intensity. The successful implementation of the quantum operations, however, requires one to provide the high precision in the durations, the frequencies, the polarizations and the strengths of the pulses together with reliable control over the delay time and the phase difference between the pulses. Besides, the use of the intermediate state lying in the neighborhood of the continuum introduces the decoherence caused by the ionization and the spontaneous emission from this state.

Here we propose the way to overcome the difficulties inherent to the electron charge manipulations by optical means. We show that the off-resonant laser pulses combined with electrostatic fields, can be used to generate an arbitrary rotation of the qubit-state vector as well as to drive an electron between the remote donors. It is essential that this method is based on the Raman-like transitions between the localized electron states of an effective molecular ion where the excited (delocalized over the double-donor system) states irrespective of their number are used as the

transport channels. As we shall see, the coherent electron dynamics is described by the simple analytical model. In order to check analytical results, we have performed numerical simulations on single-electron dynamics in the effective hydrogen molecular ion. This system is very popular object for modelling electronic properties of real donor structures (see, e.g., Refs. [18] and [20]). The eigenenergies and eigenfunctions of molecular ion were found from the stationary Schrödinger equation and then used to calculate the set of eigenfrequencies and the matrix elements of optical dipole transition between eigenstates of hydrogen molecular ion that define the field-structure interaction strengths. The time-dependent Schrödinger equation generating the coherent electron evolution in the external fields was integrated numerically for different values of structure and field parameters. By comparison of analytical expressions of the Rabi frequencies for both resonant and off-resonant cases, we found them to be in good agreement with those extracted from numerical solutions. This result confirms the validity of approximations made during the analytical treatment. The pulse and structure parameters needed for those types of quantum evolution may be evaluated from the results obtained in this study.

The paper is organized as follows. In Section II we describe general model of coherent electron dynamics in double-donor structure under the influence of near-resonant electromagnetic pulse. The Raman-like off-resonant electronic transitions are studied analytically in Section III. Besides, in this Section the possible realization of several basic single-qubit quantum operations is proposed. The results of the

numerical study of electron dynamics in hydrogen molecular ion are given in Section IV. The advantages of the off-resonant driving scheme in comparison with the resonant scheme proposed earlier as well as some questions concerned with further exploration of optically-driven donor-based charge qubits, are discussed through the Section V. We conclude our paper by Section VI.

II. MODEL

We begin with the description of the one-electron double-donor (DD) structure (Fig. 1 (a)). Let the donors A and B be placed on the axis z from each other at the distance R (hereafter - internuclear distance) large enough to consider their ground orbital states to be isolated. Due to this fact those states may be used as the qubit states $|0\rangle$ and $|1\rangle$ (for example, if an electron is localized on the donor $A(B)$, the qubit is in the state $|0\rangle$ ($|1\rangle$)). The energy difference $\Delta = \varepsilon_1 - \varepsilon_0$ may be introduced due to the structural asymmetry caused by the fabrication process and/or via the bias voltages generated by the surface gate V_a . The coupling between the excited states of individual donors through the electron tunneling gives rise to the forming of hybridized states delocalized over the DD structure. However, if $R \gg a_B^*$ (a_B^* is the effective Bohr radius of host material) the low-lying excited states are hybridized weakly and do not participate the two-donor dynamics. We shall be interested therefore only in the excited states of individual donors whose wave functions considerably overlap. The single-electron spectrum of the DD structure is presented by the sequence of the states $\{|k\rangle\}_{exc}$ which for $\Delta = 0$ are the

doublets composed of the symmetric and antisymmetric superpositions of isolated donor states. If $\Delta \neq 0$, the spectrum is assumed to be much more complex, as one can see from Fig. 1 (b). Taking into account the hydrogen-like spectrum of the isolated donors we expect the excited states close to the edge of the potential barrier separating the donors to have the quasi-continuous energy distribution.

In what follows we shall study the one-electron quantum dynamics involving the localized (qubit) states, $|0\rangle$ and $|1\rangle$, and the states $\{|k\rangle\}_{exc}$ delocalized over the structure. Our aim is to choose the field and structure parameters so that to drive an initial qubit state $|\Psi(t_0)\rangle = \alpha_0 |0\rangle + \beta_0 |1\rangle = (\alpha_0, \beta_0)^T$ into the final state $|\Psi(t)\rangle = \alpha |0\rangle + \beta |1\rangle = (\alpha, \beta)^T$ with the desired coefficients α and β .

In the absence of an external field the DD structure is characterized by the stationary Hamiltonian H_0 with the eigenstates $\{|k\rangle\}$ and the eigenenergies $\{\varepsilon_k\}$:

$$H_0 |k\rangle = \varepsilon_k |k\rangle. \quad (1)$$

The eigenstates $\{|k\rangle\}$ form the complete orthonormal set so that

$$\sum_k |k\rangle \langle k| = 1. \quad (2)$$

In the presence of the electromagnetic field the system Hamiltonian reads

$$H = H_0 - e\mathbf{E}(t) \mathbf{r}, \quad (3)$$

where e is the electron charge, $\mathbf{E}(t)$ is the field strength, \mathbf{r} is the radius-vector of an electron. With the help of Eqs. (1) and (2) we rewrite the Eq. (3) in terms of the

projection operators:

$$H = \left(\sum_k |k\rangle \langle k| \right) H \left(\sum_m |m\rangle \langle m| \right) = \sum_k \varepsilon_k |k\rangle \langle k| + \mathbf{E}(t) \sum_{k,m} \mathbf{d}_{km} |k\rangle \langle m|, \quad (4)$$

where $\mathbf{d}_{km} = \langle k| -e\mathbf{r}|m\rangle$ is the matrix element of optical dipole transition between the states $|k\rangle$ and $|m\rangle$. The state vector of the system may be presented in the form

$$|\Psi(t)\rangle = \sum_n c_n(t) e^{-i\varepsilon_n t} |n\rangle \quad (5)$$

and is governed by the non-stationary Schrödinger equation

$$i \frac{\partial |\Psi(t)\rangle}{\partial t} = H |\Psi(t)\rangle, \quad (6)$$

with the initial condition $|\Psi(t_0)\rangle = \alpha_0 |0\rangle + \beta_0 |1\rangle$ (hereafter $\hbar \equiv 1$).

Inserting Eqs. (4) and (5) into Eq. (6), we arrive at the set of linear differential equations for the probability amplitudes $c_n(t)$. We shall only examine the transitions between the states $|0\rangle$ and $|1\rangle$ and the states $\{|k\rangle\}_{exc}$:

$$\begin{aligned} i\dot{c}_0 &= \mathbf{E}(t) \sum_k \mathbf{d}_{0k} c_k e^{-i\omega_{0k}t} \\ i\dot{c}_1 &= \mathbf{E}(t) \sum_k \mathbf{d}_{1k} c_k e^{-i\omega_{1k}t} \\ i\dot{c}_k &= \mathbf{E}(t) (\mathbf{d}_{0k}^* c_0 e^{i\omega_{0k}t} + \mathbf{d}_{1k}^* c_1 e^{i\omega_{1k}t}), \quad k \in \{k\}_{exc}, \end{aligned} \quad (7)$$

where $\omega_{0(1)k} = \varepsilon_k - \varepsilon_{0(1)}$.

Let the electromagnetic field imposed on the structure to have (in the dipole approximation) the form of two phase-locked pulses

$$\mathbf{E}(t) = \mathbf{E}_0(t) \cos(\omega_0 t + \varphi_0) + \mathbf{E}_1(t) \cos(\omega_1 t + \varphi_1), \quad (8)$$

where the pulse envelopes $\mathbf{E}_0(t) = \mathbf{E}_0 f_0(t)$, $\mathbf{E}_1(t) = \mathbf{E}_1 f_1(t)$ are the slowly-varying (compared to optical frequencies) time-dependent functions, $\omega_{0,1}$ are the pulse fre-

quencies, and $\varphi_{0,1}$ are the pulse phases. We require both pulses to be in the two-photon resonance with the DD structure, i.e., $\varepsilon_0 + \omega_0 = \varepsilon_1 + \omega_1$ or, alternatively,

$$\delta_{0k} = \delta_{1k} \equiv \delta_k, \quad (9)$$

where $\delta_{0(1)k} = \omega_{0(1)} - \omega_{0(1)k}$ is the detuning of the pulse frequency $\omega_{0(1)}$ from the resonant frequency $\omega_{0(1)k}$. Note, that we use two pulses only if $\Delta \neq 0$. In the symmetric structure, where $\Delta = 0$, the single pulse $\mathbf{E}(t) = \mathbf{E}_0(t) \cos(\omega_0 t + \varphi_0)$ is enough.

Making use of the rotating-wave approximation (that implies $\Delta \ll \omega_{0(1)}$ and $|\delta_k| \ll \omega_{0(1)}$), we obtain from Eq. (7) the following set:

$$\begin{aligned} i\dot{c}_0 &= \sum_k \left[\lambda_{0k}(t) + \mu_{1k}(t) e^{-i\Delta t} \right] c_k e^{i\delta_k t} \\ i\dot{c}_1 &= \sum_k \left[\mu_{0k}(t) e^{i\Delta t} + \lambda_{1k}(t) \right] c_k e^{i\delta_k t} \\ i\dot{c}_k &= \left[\lambda_{0k}^*(t) + \mu_{1k}^*(t) e^{i\Delta t} \right] c_0 e^{-i\delta_k t} + \\ &\quad + \left[\mu_{0k}^*(t) e^{-i\Delta t} + \lambda_{1k}^*(t) \right] c_1 e^{-i\delta_k t}, \quad k \in \{k\}_{exc}, \end{aligned} \quad (10)$$

where $\lambda_{0(1)k}(t) = \lambda_{0(1)k} f_{0(1)}(t) e^{i\varphi_{0(1)}}$, $\mu_{0(1)k}(t) = \mu_{0(1)k} f_{0(1)}(t) e^{i\varphi_{0(1)}}$, $\lambda_{0(1)k} = \mathbf{d}_{0(1)k} \mathbf{E}_{0(1)} / 2$, $\mu_{0(1)k} = \mathbf{d}_{1(0)k} \mathbf{E}_{0(1)} / 2$ and the identities $\omega_{0(1)} - \omega_{1(0)k} = \delta_{1(0)k} \mp \Delta$ are used.

Eq. (10) describes the dynamical process involving many three-level excitation schemes that act in parallel. Each of them is characterized by the set of parameters Δ , $\lambda_{0(1)k}$, $\mu_{0(1)k}$, and δ_k , where $k \in \{k\}_{exc}$. We shall suppose the values of $\lambda_{0(1)k}$ and $\mu_{0(1)k}$ to be of the same order. Depending on the ratios between these parameters, k -th excitation scheme may be classified in the following way. First we consider the case of small detunings. If the coupling coefficients of the optical dipole transitions

$\lambda_{0(1)k}$ and the detunings δ_k satisfy the inequality

$$|\delta_k|, \Delta \ll |\lambda_{0k}|, |\lambda_{1k}|, \quad (11)$$

the three-level scheme works in the *resonant symmetric* regime. Instead, the applicability of the *resonant asymmetric* scheme [17] is provided by the condition

$$|\delta_k| \ll |\lambda_{0k}|, |\lambda_{1k}| \ll \Delta. \quad (12)$$

We see that the asymmetry/symmetry of the structure isn't defined by the presence/absence of the energy difference Δ only but by the ratio between Δ and the coupling coefficients $|\lambda_{0k}|, |\lambda_{1k}|$ as well. In other words, a driven DD structure can be treated (relative to the k -th transition scheme) as symmetric if the influence of the parameter Δ , introducing a "static" asymmetry, is compensated by an appropriate value of the field strength defined from (11). In this case only one external pulse is sufficient to excite both transitions [21].

Next we shall examine the opposite case where the states $|0\rangle$ and $|1\rangle$ are connected through the off-resonant transitions involving a collection of the excited states lying at the edge of the potential barrier. Two situations are possible again:

$$\Delta \ll |\lambda_{0k}|, |\lambda_{1k}| \ll |\delta_k| \quad (13)$$

and

$$|\lambda_{0k}|, |\lambda_{1k}| \ll |\delta_k|, \Delta. \quad (14)$$

The first of these inequalities corresponds to the *off-resonant symmetric* excitation scheme. This situation was studied in Refs. [22, 23] for the double-dot structures

with three and four levels. As it was shown, the set of single-qubit operations produced by such one-electron dynamics is incomplete, since in order to realize an arbitrary rotation of the qubit-state vector, the structure symmetry must be broken. In what follows, our attention will be focused on both the symmetric case and the *off-resonant asymmetric* case for which the conditions (14) are satisfied and each pulse drives the transitions between only one of localized state and the transport states $\{|k\rangle\}_{exc}$. This implies also that the values of Δ and δ_k must be rather different from each other for all k to prevent the single-donor resonant dynamics.

III. THE OFF-RESONANT DYNAMICS

In this Section we consider two cases of the off-resonant electronic quantum dynamics in DD structure, i.e., the off-resonant symmetric dynamics and the off-resonant asymmetric dynamics. We begin with the second one, initially specifying the conditions imposed on pulse and structure parameters:

$$|\lambda_{0(1)k}|, |\mu_{0(1)k}| \ll \Delta \ll |\delta_k|; \left| \frac{\partial}{\partial t} \lambda_{0(1)k} \right|, \left| \frac{\partial}{\partial t} \mu_{0(1)k} \right| \ll |\lambda_{0(1)k}|^2, |\mu_{0(1)k}|^2. \quad (15)$$

(The case of large Δ is out of scope of this study; see Sec. IV D for the reasons).

Strictly speaking, the rotating-wave approximation used in derivation of Eq. (10) and based on the averaging of Eq. (7) over time interval $[\tau - \pi/\omega_0, \tau + \pi/\omega_0]$ (RWA 1) [24], cannot be applied to high-lying states for which the detunings δ_k become comparable to the pulse frequencies. Let us define effective "maximal" detuning $\delta_{\max} \leq \omega_0$ that corresponds to the upper bound of energy range, where RWA 1 is still valid, and average Eq. (10) over time interval $[\tau - \pi/\delta_{\max}, \tau + \pi/\delta_{\max}]$ (RWA

2). This step is justified by first of the inequalities (15). After some manipulations,

we obtain two equations for time-averaged functions c_0 and c_1 :

$$\begin{aligned} i\dot{c}_0 &= \sum_k \frac{1}{\delta_k} \left\{ |\lambda_{0k} + \mu_{1k} \exp(-i\Delta \cdot t)|^2 c_0 + [\lambda_{0k} + \mu_{1k} \exp(-i\Delta \cdot t)] [\lambda_{1k} + \mu_{0k} \exp(i\Delta \cdot t)]^* c_1 \right\}, \\ i\dot{c}_1 &= \sum_k \frac{1}{\delta_k} \left\{ |\lambda_{1k} + \mu_{0k} \exp(i\Delta \cdot t)|^2 c_1 + [\lambda_{0k} + \mu_{1k} \exp(-i\Delta \cdot t)]^* [\lambda_{1k} + \mu_{0k} \exp(i\Delta \cdot t)] c_0 \right\}. \end{aligned} \quad (16)$$

Again, careful consideration of averaging procedure requires us to handle only with the detunings that are sufficiently small in comparison with δ_{\max} . It is easy to see that the equations (16) do not contain the fast-oscillating terms $c_{k \neq 0,1}$. Therefore, these equations describe effective two-state dynamics involving only the localized states $|0\rangle$ and $|1\rangle$. From third equation of the set (10) we conclude that the functions $c_{k \neq 0,1}$ have the amplitudes $\sim |\lambda_{0k}/\delta_k| \ll 1$ and oscillate at the frequencies $\sim |\delta_k|$. The reduction of set like Eq. (10) to the two equations for slowly-varying probability amplitudes c_0 and c_1 is known in atomic optics as the adiabatic elimination procedure [25] - [27]. To proceed further, let us average the equations (16) over the time interval $[\tau - \pi/\Delta, \tau + \pi/\Delta]$ (RWA 3) on which all of the time-dependent functions except $\exp(\pm i\Delta t)$ may be replaced by their mean values so that after integration we arrive at the following set of equations:

$$\begin{aligned} i\dot{c}_0 &= \sum_k \frac{1}{\delta_k} \left\{ [|\lambda_{0k}(t)|^2 + |\mu_{1k}(t)|^2] c_0 + \lambda_{0k}(t) \lambda_{1k}^*(t) c_1 \right\}, \\ i\dot{c}_1 &= \sum_k \frac{1}{\delta_k} \left\{ \lambda_{0k}^*(t) \lambda_{1k}(t) c_0 + [|\lambda_{1k}(t)|^2 + |\mu_{0k}(t)|^2] c_1 \right\}. \end{aligned} \quad (17)$$

Now we return to the symmetric driving scheme that is simpler than the asymmetric one. By setting $\Delta = 0$ and $\mathbf{E}_1 = 0$, we transform the set of Eq. (10)

into

$$\begin{aligned} i\dot{c}_0 &= \sum_k \lambda_{0k}(t) b_k \\ i\dot{c}_1 &= \sum_k \lambda_{1k}(t) b_k \\ i\dot{b}_k &= -\delta_k b_k + \lambda_{0k}^*(t) c_0 + \lambda_{1k}^*(t) c_1, \quad k \in \{k\}_{exc}, \end{aligned} \quad (18)$$

where $b_k = c_k \exp(i\delta_k t)$, $k \in \{k\}_{exc}$ and we redefine the coupling coefficients as $\lambda_{0(1)k}(t) = \lambda_{0(1)k} f_0(t) e^{i\varphi_0}$, $\lambda_{0(1)k} = \mathbf{d}_{0(1)k} \mathbf{E}_0 / 2$. The inequalities (13) allow one to apply the adiabatic elimination procedure to the intermediate levels $\{|k\rangle\}_{exc}$:

$$\dot{b}_k \approx 0, \quad b_k \approx [\lambda_{0k}^*(t) c_0 + \lambda_{1k}^*(t) c_1] / \delta_k, \quad k \in \{k\}_{exc}. \quad (19)$$

The equations for two remaining probability amplitudes c_0 and c_1 in the matrix form for both asymmetric and symmetric dynamics read

$$i \frac{\partial}{\partial t} \begin{pmatrix} c_0 \\ c_1 \end{pmatrix} = \begin{pmatrix} \Lambda_0(t) & \Lambda_2(t) \\ \Lambda_2^*(t) & \Lambda_1(t) \end{pmatrix} \begin{pmatrix} c_0 \\ c_1 \end{pmatrix}, \quad (20)$$

where for symmetric case one has $\Lambda_0(t) = \Lambda_0 f_0^2(t)$, $\Lambda_1(t) = \Lambda_1 f_0^2(t)$, $\Lambda_2(t) = \Lambda_2 f_0^2(t)$ and

$$\Lambda_0 = \sum_k |\lambda_{0k}|^2 / \delta_k, \quad \Lambda_1 = \sum_k |\lambda_{1k}|^2 / \delta_k, \quad \Lambda_2 = \sum_k \lambda_{0k} \lambda_{1k}^* / \delta_k, \quad (21)$$

whereas for asymmetric case the functions entering into Eq. (20) are given by expressions $\Lambda_0(t) = \sum_k [|\lambda_{0k}(t)|^2 + |\mu_{1k}(t)|^2] / \delta_k$, $\Lambda_1(t) = \sum_k [|\lambda_{1k}(t)|^2 + |\mu_{0k}(t)|^2] / \delta_k$, and $\Lambda_2(t) = \sum_k \lambda_{0k}(t) \lambda_{1k}^*(t) / \delta_k$. It allows us to treat both cases in the same manner, however, keeping in mind that for symmetric structure $\Lambda_0(t) = \Lambda_1(t)$, since $\lambda_{0k} = \pm \lambda_{1k}$ for the state $|k\rangle$ whose electronic wave function possesses even/odd parity relative to the center of DD structure, that does not take place for asymmetric

structure. Below we present the general solution of Eq. (20) that will describe both types of off-resonant electron dynamics.

The eigenstates and the eigenenergies of the matrix in right-hand side of Eq. (20) may be written as

$$\begin{cases} |+\rangle = e^{i \arg[\Lambda_2(t)]} \cos [\Theta(t)/2] |0\rangle + \sin [\Theta(t)/2] |1\rangle \\ |-\rangle = e^{i \arg[\Lambda_2(t)]} \sin [\Theta(t)/2] |0\rangle - \cos [\Theta(t)/2] |1\rangle \end{cases} \quad (22)$$

and

$$E_{\pm}(t) = [\Lambda_0(t) + \Lambda_1(t)]/2 \pm \Omega(t), \quad (23)$$

respectively, where

$$\cos [\Theta(t)] = [\Lambda_0(t) - \Lambda_1(t)]/2\Omega(t), \quad \sin [\Theta(t)] = |\Lambda_2(t)|/\Omega(t), \quad (24)$$

and

$$\Omega(t) = \sqrt{[\Lambda_0(t) - \Lambda_1(t)]^2/4 + |\Lambda_2(t)|^2} \quad (25)$$

is the instantaneous Rabi frequency. Using the unitary transformation

$$D(t) = \begin{pmatrix} e^{i \arg[\Lambda_2(t)]} \cos [\Theta(t)/2] & e^{i \arg[\Lambda_2(t)]} \sin [\Theta(t)/2] \\ \sin [\Theta(t)/2] & -\cos [\Theta(t)/2] \end{pmatrix} \quad (26)$$

we represent the state vector in the instantaneous basis $\{|+\rangle, |-\rangle\}$ as

$$|\Phi(t)\rangle = a_+(t) |+\rangle + a_-(t) |-\rangle, \quad |\Psi(t)\rangle = D(t) |\Phi(t)\rangle \quad (27)$$

and rewrite Eq. (20) in the new basis as

$$i \frac{\partial}{\partial t} \begin{pmatrix} a_+ \\ a_- \end{pmatrix} = \begin{pmatrix} E_+ & \dot{\Theta}/2 \\ -\dot{\Theta}/2 & E_- \end{pmatrix} \begin{pmatrix} a_+ \\ a_- \end{pmatrix}, \quad (28)$$

where

$$\dot{\Theta}(t) = \frac{|\dot{\Lambda}_0(t) - \dot{\Lambda}_1(t)| |\Lambda_2(t)| - |\dot{\Lambda}_2(t)| |\Lambda_0(t) - \Lambda_1(t)|}{[\Lambda_0(t) - \Lambda_1(t)]^2/4 + |\Lambda_2(t)|^2}. \quad (29)$$

Here we restrict our interest by the diagonal evolution followed from the choice of the system parameters for which $\dot{\Theta}(t) \ll E_{\pm}(t)$. In this case the solution of Eq. (28) is straightforward:

$$\begin{aligned} a_+(t) &= a_+(t_0) \exp \left[-i \int_{t_0}^t E_+(t') dt' \right], \\ a_-(t) &= a_-(t_0) \exp \left[-i \int_{t_0}^t E_-(t') dt' \right]. \end{aligned} \quad (30)$$

With the help of equations (26), (27), and (30) we may write down the expression for the evolution matrix of the qubit-state vector $|\Psi(t)\rangle$ in the laboratory frame:

$$\begin{aligned} |\Psi(t)\rangle &= U |\Psi(t_0)\rangle, \\ U &= \begin{pmatrix} e^{-i\varepsilon_0 t} & 0 \\ 0 & e^{-i\varepsilon_1 t} \end{pmatrix} D(t) \begin{pmatrix} e^{-i \int_{t_0}^t E_+(t') dt'} & 0 \\ 0 & e^{-i \int_{t_0}^t E_-(t') dt'} \end{pmatrix} D^\dagger(t_0) = \\ &= e^{-i[\varepsilon_0 t + \varphi_\Lambda(t)]} \begin{pmatrix} u_{00} & u_{01} \\ u_{10} e^{-i\Delta t} & u_{11} e^{-i\Delta t} \end{pmatrix}, \end{aligned} \quad (31)$$

where

$$\begin{aligned} u_{00} &= u_{11}^* = e^{-i\tilde{\Omega}(t)} \cos[\Theta(t)/2] \cos[\Theta(t_0)/2] + e^{i\tilde{\Omega}(t)} \sin[\Theta(t)/2] \sin[\Theta(t_0)/2], \\ u_{01} &= -u_{10}^* = \\ &= e^{i \arg[\Lambda_2(t)]} \left\{ e^{-i\tilde{\Omega}(t)} \cos[\Theta(t)/2] \sin[\Theta(t_0)/2] - e^{i\tilde{\Omega}(t)} \sin[\Theta(t)/2] \cos[\Theta(t_0)/2] \right\}, \end{aligned} \quad (32)$$

and

$$\tilde{\Omega}(t) = \int_{t_0}^t \Omega(t') dt', \quad \varphi_\Lambda(t) = \int_{t_0}^t [\Lambda_0(t') + \Lambda_1(t')]/2 dt'. \quad (33)$$

The expressions (31) - (33) describe the effective two-level dynamics that corresponds to the continuous evolution of the qubit state vector on the Bloch sphere. In the

remainder of this section we show how to choose the pulse and structure parameters in order to realize the most important single-qubit gates. We illustrate the qubit state engineering by considering a particular case of the driving pulses sharing the same time dependence, i.e., $f_0(t) = f_1(t) \equiv f(t)$. The condition $\dot{\Theta} = 0$ is then satisfied and the components of the evolution matrix (31) take the form

$$\begin{aligned} u_{00} &= u_{11}^* = \cos[\tilde{\Omega}(t)] - i \cos(\Theta_0) \sin[\tilde{\Omega}(t)], \\ u_{01} &= -u_{10}^* = -ie^{i \arg(\Lambda_2)} \sin(\Theta_0) \sin[\tilde{\Omega}(t)], \end{aligned} \quad (34)$$

where $\Theta_0 = \arcsin \left[|\Lambda_2| / \sqrt{(\Lambda_0 - \Lambda_1)^2 / 4 + |\Lambda_2|^2} \right]$. The dynamics described by the equations (34) is sufficient to generate an arbitrary single-qubit rotation on the Bloch sphere. For example, the quantum operations such as NOT (σ_x): $(\alpha_0, \beta_0)^T \rightarrow (\beta_0, \alpha_0)^T$; PHASE (σ_z): $(\alpha_0, \beta_0)^T \rightarrow (\alpha_0, -\beta_0)^T$; and Hadamard (H): $(\alpha_0, \beta_0)^T \rightarrow [(\alpha_0 + \beta_0)/\sqrt{2}, (\alpha_0 - \beta_0)/\sqrt{2}]^T$ can be realized (up to the common phase) given the following choices of the pulse - structure parameters:

$$\tilde{\Omega}(T) = \pi/2 + \pi k, \quad T\Delta = 2\pi l, \quad \arg(\Lambda_2) = 2\pi m \quad (35)$$

and

$$\Theta_0(\sigma_x) = \pi/2 + 2\pi n, \quad \Theta_0(\sigma_z) = \pi n, \quad \Theta_0(H) = \pi/4 + \pi n, \quad (36)$$

respectively. Here k, l, m , and n are the integers and T is the pulse duration. Of course, this is not a unique parameter choice to attain the above quantum operations. Careful estimation of the operation times requires the detailed knowledge of the energy spectrum of DD structure and the values of $\lambda_{0(1)k}$.

IV. A HYDROGEN MOLECULAR ION: NUMERICAL STUDY

We visualize our results with the help of model, where the energies and wave functions of an electron, bounded in the DD structure, are approximated by the eigenenergies and eigenfunctions of effective hydrogen molecular ion H_2^+ , for which the effective Bohr radius $a_B^* = \epsilon(m_0/m^*)a_B$ and the effective Rydberg energy $Ry^* = [m^*/(\epsilon^2 m_0)]Ry$ contain the information about real solid-state environment via the electronic effective mass m^* and the dielectric constant ϵ ($Ry = 13.6057$ eV is Rydberg energy, $a_B = 0.5292 \times 10^{-10}$ m is the Bohr radius, and $m_0 = 9.1094 \times 10^{-31}$ kg is the free electron mass). In practice, the single-valley approximation was applied to study the phonon-induced decoherence of electron in $Si:P_2^+$ structure [20] and the effect of surface gate on single phosphorous donor in the silicon [28], as well as to calculate the Rabi frequency of resonant electron transfer between localized states in $Si:P_2^+$ structure in three-level approximation [18]. The comparison of the results of calculations, where intervalley interference is taken into account, with those neglecting such effects, demonstrates qualitative agreement between them (especially in presence of an external field, see [16]). In our study, we are mostly interested in validation of the approximations, made during the paper to reveal the specific features of resonant and off-resonant electron dynamics in a multilevel structure. We expect, that the dynamical analysis developed above and confirmed numerically below for effective single-valley-approximated structure, can be applied to real solid-state DD structures as well.

In what follows we show how to find the eigenenergies and eigenfunctions of

hydrogen molecular ion (HMI) without LCAO approximation. We calculate the matrix elements of optical dipole transition and study their behavior under axial electric field. We shall work with atomic units (a.u.), keeping for energy $1 \text{ a.u.} = 2Ry^* = E_D$ (E_D is the effective ionization energy) and for distance $1 \text{ a.u.} = a_B^*$.

A. Eigenenergies and eigenfunctions of HMI at zero bias field

There exist several ways how to compute the eigenenergies and eigenfunctions of HMI. We consider one of them using variable separation in the time-independent Schrödinger equation followed by representation of solution in new variables via appropriate series expansions (see the work [29] and references therein). It is well known that the Schrödinger equation for HMI

$$\left(\frac{1}{2}\nabla^2 + E + \frac{1}{r_A} + \frac{1}{r_B}\right)\Psi(\mathbf{r}) = 0, \quad (37)$$

where $r_{A(B)}$ denotes the distance between an electron and atom $A(B)$, is separable in prolate spheroidal coordinates $\xi = (r_A + r_B)/R$, $\eta = (r_A - r_B)/R$, $\varphi = \arctan(y/x)$ ($1 \leq \xi \leq \infty$, $-1 \leq \eta \leq 1$, $0 \leq \varphi \leq 2\pi$) and a (non-normalized) stationary electronic wave function of HMI can be written in the form $\Psi(\xi, \eta, \varphi) = \Xi(\xi)H(\eta)\Phi(\varphi)$, where functions $\Xi(\xi)$ and $H(\eta)$ meet the generalized radial and angular spheroidal wave equations, respectively, and the azimuthal function $\Phi(\varphi)$ is the same as for hydrogen atom: $\Phi(\varphi) = \exp(im\varphi)/\sqrt{2\pi}$, where $m = 0, \pm 1, \pm 2, \dots$ is the azimuthal (or magnetic) quantum number. The most useful expansion for $H(\eta)$ is in a series of associated Legendre polynomials, whereas for $\Xi(\xi)$ the power series expansion is applied. Substituting these functions into corresponding wave equa-

tions and requiring them to be minimal solutions of these equations, we obtain the expansion coefficients and separation constants C_ξ and C_η that at fixed m depend continuously on the energy parameter E and on the internuclear distance R . To obtain electronic eigenenergies we now have to find the set of separation constants common for both radial and angular solutions for given m and R . Graphically, these can be sought as intersection points of curves from sets $\{C_\xi(E)\}$ and $\{C_\eta(E)\}$ and corresponding values of parameter E will be the eigenenergies of HMI (for more details, see the Ref. [29]).

The HMI eigenstates is completely specified by the set of quantum numbers (N_ξ, N_η, m) , where $N_\xi(N_\eta)$ equals to the number of zeros in radial (angular) function $\Xi(\xi)$ ($H(\eta)$). On the other hand, in the united atom limit $R \rightarrow 0$ the quantum numbers (n_u, l, m) are used, where n_u specifies the energy level, and l the angular momentum. Both sets are related by the formulas $N_\xi = n_u - l - 1$, $N_\eta = l - m$. In what follows we shall use the second one for the state classification as more instructive, i.e., $\Psi(\xi, \eta, \varphi) \leftrightarrow |n_u l m\rangle$. According to standard atomic notation, the letters s, p, d, f, g, h, \dots are used to denote the values of $l = 0, 1, 2, 3, \dots$ in united atom limiting case, and the greek letters $\sigma, \pi, \delta, \phi, \dots$ denote the values of m . We can also classify the states of homonuclear HMI by the parity under the transformation $\mathbf{r} \rightarrow -\mathbf{r}$, namely, the state with symmetrical (antisymmetrical) wave function will be supplied with subscript g (u).

Making use of computational framework sketched above, we have found the eigenen-

ergies and eigenfunctions of discrete part of HMI energy spectrum. At Fig. 2, the eigenenergies of first 20 σ -states ($m = 0$) are plotted as functions of internuclear distance R for $20 < R < 40$ (on the whole, we found the eigenenergies of 64 states with $m = 0$). We also computed the eigenenergies of states from subspaces with $m \neq 0$, however, only σ -states are relevant for the dynamical description of electron evolution in the electric fields polarized along z axis that will be in the focus of further consideration. The HMI eigenenergies are found with absolute accuracy 10^{-15} a.u. that is enough for this study, but the described algorithm enables one to calculate them with absolute accuracy 10^{-20} a.u. or even higher [29]. From Fig. 2 (a) it is seen that two low-lying states of HMI, i.e., $|1s\sigma_g\rangle$ and $|2p\sigma_u\rangle$, are almost degenerate, and the energy difference $\Delta_{1s\sigma_g-2p\sigma_u} = \varepsilon(2p\sigma_u) - \varepsilon(1s\sigma_g)$ decreases exponentially with R . The dependence of the electronic tunneling time $\tau_{1s\sigma_g-2p\sigma_u} = \hbar / \Delta_{1s\sigma_g-2p\sigma_u}$ (here $\hbar = 6.582 \times 10^{-16}$ eV \times s) between these states on R can be seen at Fig. 3, where the parameters $E_D = -45$ meV and $a_B^* = 1.22$ nm, taken from Ref. [16] for Si:P₂⁺ in single valley approximation, are used. From this Figure we obtain an estimation on $\tau_{1s\sigma_g-2p\sigma_u}$ for $R \approx 30$ nm (≈ 20 a.u.) to be of order of 1 μ s that is enough for carrying out some proof-of principle experiments, whereas for $R \approx 50$ nm (≈ 40 a.u.) one has for the tunneling time $\tau_{1s\sigma_g-2p\sigma_u} \approx 10^2$ s that would enable to run quantum algorithms. The states $|1s\sigma_g\rangle$ and $|2p\sigma_u\rangle$ are presented by even and odd superpositions of states localized on donors A and B . Inversely, the logical (localized) states can be expressed by even and odd superpositions of the states $|1s\sigma_g\rangle$ and $|2p\sigma_u\rangle$ of

$$\text{HMI: } |0(1)\rangle = |1s^{A(B)}\rangle = (|1s\sigma_g\rangle \pm |2p\sigma_u\rangle)/\sqrt{2}.$$

The collection of low-lying electronic excited states falls into the subbands characterized at $R \gg 1$ by the principal quantum number n of isolated hydrogen atom. The sets of HMI eigenstates, whose energies are pictured at Fig. 2 (b), namely, $\{|4f\sigma_u\rangle, |3d\sigma_g\rangle, |3p\sigma_u\rangle, |2s\sigma_g\rangle\}$, $\{|6h\sigma_u\rangle, |5g\sigma_g\rangle, |5f\sigma_u\rangle, |4d\sigma_g\rangle, |4p\sigma_u\rangle, |3s\sigma_g\rangle\}$, and $\{|7j\sigma_u\rangle, |6h\sigma_g\rangle, \dots\}$ (not labelled), correspond to $n=2$, $n=3$, and $n=4$, respectively. In their turn, these subbands can be subdivided further into the doublets $|k s \sigma_g\rangle - |(k+1) p \sigma_u\rangle$, $k=2,3,\dots$; $|k d \sigma_g\rangle - |(k+1) f \sigma_u\rangle$, $k=3,4,\dots$; and so on. The degree of hybridization/localization can be evaluated from state quantum numbers. For example, the pairs of states with $l = s, p$ become degenerate at comparatively small internuclear distances. The doublets of states with $l = d, f$ are well resolved up to $R \approx 30$ and collapse quickly for larger R . We observe almost complete dissociation of HMI states, pertaining to the subband with $n=2$, into two pairs of states $|2s^{A(B)}\rangle = (|2s\sigma_g\rangle \pm |3p\sigma_u\rangle + |3d\sigma_g\rangle \pm |4f\sigma_u\rangle)/2$ and $|2p\sigma^{A(B)}\rangle = (|2s\sigma_g\rangle \pm |3p\sigma_u\rangle - |3d\sigma_g\rangle \mp |4f\sigma_u\rangle)/2$ of isolated hydrogen atoms. Taking the average over the energies of states pertaining to the subbands with $n=1$ and $n=2$ and adding the energy of internuclear repulsion $\varepsilon_{nucl} = 1/R$, we arrive at isolated hydrogen atom energies $\varepsilon(n) = 1/2n^2$. On the other hand, the states with higher values of l remain non-degenerate on the whole interval of R under consideration. One can therefore treat those states as reliable transport channels to drive an electron between logical states. As we shall see below, the states $|5g\sigma_g\rangle$ and $|6h\sigma_u\rangle$ (whose

energies are plotted as thick red lines at Fig. 2 (b)) meet the conditions imposed on the choice of transport states by the high excitation selectivity and appropriate dipole coupling strength requirements. The states, whose energies are plotted as thick blue lines, may be exploited as transport ones either at $R < 20$ ($|3d\sigma_g\rangle$ and $|4f\sigma_u\rangle$) or at $R > 30$ ($|6g\sigma_g\rangle$, $|7h\sigma_u\rangle$, $|7i\sigma_g\rangle$).

B. Matrix elements of optical dipole transition at zero bias field

The numerical solution of Eq. (6) implies the knowledge of matrix elements $\{\mathbf{d}_{km}\}$ of optical dipole transition (ODT) between all states entering into the Eq. (4). In our simulation we restrict ourselves by consideration of electric fields polarized along z axis, so that the field-structure interaction Hamiltonian in Eq. (3) reads $-eE(t)z$. In this case, the matrix elements of ODT between states $|k\rangle$ and $|m\rangle$ can be calculated in spheroidal coordinates through the expression

$$d_{km} = \frac{1}{\sqrt{N_k N_m}} \left\{ \int_{-1}^1 d\eta \int_1^\infty d\xi [\mathbf{H}_k(\eta) \Xi_k(\xi)] (-eR\xi\eta/2) [\mathbf{H}_m(\eta) \Xi_m(\xi)] J(\xi, \eta) \right\}, \quad (38)$$

$$N_{k(m)} = \int_{-1}^1 d\eta \int_1^\infty d\xi [\mathbf{H}_{k(m)}(\eta) \Xi_{k(m)}(\xi)]^2 J(\xi, \eta), \quad J(\xi, \eta) = \xi^2 - \eta^2, \quad (39)$$

where $J(\xi, \eta)$ is the Jacobian of the transformation from cartesian frame to spheroidal frame, and the relation $z = (R/2)\xi\eta$ is used. (The wave functions $\mathbf{H}_{k(m)}(\eta)$ and $\Xi_{k(m)}$ of discrete part of HMI energy spectrum are real functions, hence the ODT matrix elements will be real as well). According to the selection rule $\Delta m = 0$, imposed by the structure axial symmetry and by the choice of the field polarization, and keeping in mind that logical states pertain to the σ -subspace of HMI eigenstates,

only the transitions among the states with $m = 0$ are relevant. Besides, the analysis of Eq. (38) supplies us with other selection rule standing for allowed transitions Δl to be an odd number. In other words, the states from subspaces $\{s, d, g, i, \dots\}$ with even l are dipole-coupled to the states from subspaces $\{p, f, h, j, \dots\}$ with odd l . It means that ODT selection rule upon l , that follows from spatial symmetry of HMI, turns out to be relaxed in comparison with that of hydrogen-like atom for which $\Delta l = \pm 1$.

Using the equations (38) and (39), we have calculated the ODT matrix elements between all pairs of 64 low-lying σ -states of HMI as functions of internuclear distance R . In what follows, they will be used to define the right-hand side of Eq. (6). At the same time, in Eq. (21) we proceed with matrix elements between logical states $|0\rangle$ and $|1\rangle$ and excited ones. These matrix elements can be derived from expression $d_{0(1)k} = (d_{1s\sigma_g k} \pm d_{2p\sigma_u k})/\sqrt{2}$. The dependencies of d_{0k} (1 a.u. = ea_B^*) on R are given at Figs. 4 (a) - (c) for subbands with $n = 2, 3, 4$. Note that in symmetric HMI $d_{0k} = d_{1k}$, if k denotes a state with even parity, and $d_{0k} = -d_{1k}$, if k denotes a state with odd parity. The calculation of matrix elements between localized states $|1s^{A,B}\rangle$ from subband with $n = 1$ (logical subspace) and localized states $|2s^{A,B}\rangle$ and $|2p\sigma^{A,B}\rangle$ from subband with $n = 2$, yields at $R = 38$ $d_{1s-2s}^{A,B} \approx 0$ and $d_{1s-2p\sigma}^{A,B} \approx 0.746$ that coincide with values $d_{z1s-2s} = 0$ and $d_{z1s-2p\sigma} = \frac{2^8}{3^5\sqrt{2}}(ea_B^*) \approx 0.745$ for hydrogen atom.

C. Resonant and off-resonant electron dynamics in zero-bias case

Here we present the results of numerical simulations on coherent electron evolution, paying attention to performing σ_X qubit-state vector rotation. For simplicity, we work with square pulses and $f(t)$ entering into Eq. (34) is the step function. To drive an electronic population in symmetric structure such as HMI, a single pulse is only needed, thus we integrate Eq. (6) with Hamiltonian $H = H_0 - eE_0 z \cos(\omega_0 t)$, and initial conditions corresponding to the localization of an electron into logical state $|0\rangle$, are $c_{1s\sigma_g}(0) = c_{2p\sigma_u}(0) = 1/\sqrt{2}$. Our goal is to calculate the frequencies of Rabi oscillations between logical states and to estimate the degree of population leakage from logical subspace for different values of internuclear distance R , pulse strength E_0 , and pulse frequency ω_0 . For this purpose, we analyze the probabilities $p_0(T)$ and $p_1(T)$ ($p_{0(1)}(T) = |c_{1s\sigma_g}(T) \pm c_{2p\sigma_u}(T)|^2/2$) to find electron into the logical states $|0\rangle$ and $|1\rangle$, together with total probability $p_{tr}(T) = \sum_{k \neq 0,1} p_k(T)$ of electron to be out of logical subspace, versus the pulse duration T .

Let us introduce the dimensionless field energy $\varepsilon_{field} = eE_0 a_B^*/2Ry^*$ and the dimensionless pulse duration $T = 2Ry^*t/\hbar$. According to the analysis given in Sec. II, the coupling coefficients that in atomic units take the form $\lambda_{0(1)k} = \varepsilon_{field} d_{0(1)k}/2$, have to satisfy the requirements imposed by a concrete optical excitation regime. If one applies a resonant driving scheme, where HMI state $|r\rangle$ is used as transport state, the detuning of pulse frequency ω_0 from resonant frequency ω_{0r} must be much smaller than the value of coupling coefficient $|\lambda_{0r}|$. In its turn, $|\lambda_{0r}|$ must be much smaller than ω_{rr+1} and ω_{r-1r} in order to minimize population leakage into the

states nearest-in-energy to transport state. Instead, the exploitation of strongly-detuned pulses (Raman scheme) implies the values of coupling coefficients $|\lambda_{0k}|$ for all excited states to be much smaller than corresponding detunings. It is easy to see that one could attain this condition taking pulse strength as small as possible and detunings as large as possible. However, this brings about considerable reduction in Rabi frequency. In so far, we shall be interested in determination of optimal pulse parameter set, that would amount to rapid and robust implementation of quantum operations.

We begin with resonant driving scheme that, being realized in symmetric structure, may be considered as auxiliary one, since it is only able to inverse the population of logical states at discrete set of pulse durations when the electron is concentrated into logical subspace. The electronic resonant population transfer in three-level and in four-level structures was studied theoretically in Refs. [21] and [23], where the probabilities p_0 , p_1 , and p_{tr} were found at exact resonance (zero detuning from transport level) to be

$$p_0(T) = \cos^4\left(\frac{E_0 d_{0tr} T}{4}\right), \quad p_1(T) = \sin^4\left(\frac{E_0 d_{0tr} T}{4}\right), \quad p_{tr}(T) = \frac{1}{2} \sin^2\left(\frac{E_0 d_{0tr} T}{2}\right). \quad (40)$$

One can observe from Fig. 5 that these expressions are in excellent agreement with numerical curves. We have performed our simulations on resonant dynamics for several values of ε_{field} (different pulse strengths E_0) and pulse frequencies ω_0 , matching resonant frequencies of HMI (different d_{0tr}) in order to define the dependency of Rabi

frequency on these parameters. We have revealed that the pulses with $\varepsilon_{field} < 0.003$ being tuned on resonance with states $|5g\sigma_g\rangle$ or $|6h\sigma_u\rangle$, provide good selectivity, low population leakage at the end of NOT operation ($p_1(T_{NOT} = \pi/2\Omega_R) > 0.999$), and quite high speed of electronic transfer ($T_{NOT} \approx 10^4$ that is of order of hundreds of picoseconds for Si:P₂⁺ structure). We have also performed numerical simulations on the electron dynamics for $R = 22$ in order to check the possibility of using the states from HMI subband with $n = 2$ as transport ones. As it was expected, the resonant population transfer between logical states via excitation of one of the states $\{|3d\sigma_g\rangle, |4f\sigma_u\rangle\}$ do really take place. However, large dipole moments for those transitions (see Fig. 4 (a)) require the field energy to be sufficiently low since the energy spacings between subband levels are still small. As a result, the time needed for complete electron transfer is of the same order as it was for larger R , where the states from third and fourth subbands, characterized by smaller values of ODT matrix elements but demonstrating higher resolution over energy, play role of transport channels. Thus the formula $\Omega_R = |E_0 d_{0tr}|/4 = |\lambda_{0tr}|/2$ approximates with high accuracy the Rabi frequency for resonant electronic transfer for $20 < R < 40$.

Now we present the results of calculations for the off-resonant scheme. Typical curves for p_0 , p_1 , and p_{tr} , reflecting coherent electron dynamics driven by strongly detuned pulses, are plotted at Fig. 6. They demonstrate essentially two-level oscillatory behavior where the population is mainly localized in logical subspace. This picture differs from that obtained for resonant scenario by sharp decrease in the

amplitude of population p_{tr} combined with considerable increase in the oscillation period of p_0 and p_1 (by order of magnitude or more). According to Eqs. (21), (31), (33) and (34), in the symmetric structure $\Lambda_0 - \Lambda_1 = 0$, $\Theta_0 = \pi/2$, and

$$p_0(T) \approx \cos^2(\Omega_R T), \quad p_1(T) \approx \sin^2(\Omega_R T), \quad (41)$$

where $\Omega_R = |\Lambda_2|$ (see Eq. (25)). Relative to the transport states, we are only able to estimate under adiabatic elimination an order of magnitude of total probability as $p_{tr} \sim (\lambda_{0k}/\delta_{0k})_{\max}^2 \ll 1$ and its oscillation frequency $\Omega_{tr} \sim (\delta_{0k}^2/\lambda_{0k})_{\max} \gg \Omega_R$, so that p_{tr} exhibits fast oscillations with small amplitude.

In order to compare the Rabi frequencies found numerically with those calculated within analytical framework, we plot both data types on Fig. 7 versus pulse frequency (shifted by ε_0) for $R = 30$ and $R = 38$ and for the field energies $\varepsilon_{field}=0.003$ and $\varepsilon_{field}=0.005$. To extract numerical values of $|\Lambda_2|$, we fit the curves for $p_1(T)$ by squared sine function and then define Ω_R as the sine frequency. These values, drawn as filled circles, correlate well with analytical results of Eq. (21) pictured by solid curves. Since the approximation applied in derivation of Eqs. (20) and (21) do not allow one to work in near neighborhood of HMI energy levels, we have left empty the intervals around the levels marking them by vertical dotted lines. We shall regard the oscillations as two-level ones if the depth of modulations of p_0 and p_1 , arising from the non-resonant population of excited states, is smaller than 0.01. At Fig. 7, there are several points (enclosed by open red squares) satisfying to this conventional criterion. Other numerical data points correspond to the p_{tr} maxima (or modula-

tion depths) ranging from 0.01 to 0.05. For the points located at the boundaries of the intervals, on which approximate solution is valid, the maximum values of p_{tr} turn out to be 0.05 or higher. With further approaching of the pulse frequency to one of HMI resonant frequencies, the off-resonant oscillatory picture transforms into resonant one. The off-resonant dynamics at $R = 22$ (not shown) is quite similar to that presented at Fig. 7. Again, almost ideal two-level oscillations are obtained if we tune the pulse frequency into the middle of doublet $\{|5g\sigma_g\rangle, |6h\sigma_u\rangle\}$. With that, the use of doublet $\{|3d\sigma_g\rangle, |4f\sigma_u\rangle\}$ becomes possible provided that the pulse strength is not high ($\varepsilon_{field} \leq 0.001$). As it will be shown below, we cannot efficiently operate with such pulses since the Rabi frequency of qubit rotations appears to be very small.

Note that the character of oscillations of total population of excited states is regular enough in both resonant and off-resonant cases; this observation can be explained by assumption that only several excited states participate the dynamics. Such an explanation is obvious for resonant excitation scheme, but in off-resonant case, where all excited states are equivalent in dynamical sense, rigorous arguments are needed. To find them, let us consider the sum Λ_2 in more details. As we have mentioned before, the excited states of HMI can be classified by tunnel coupling strength between symmetric and antisymmetric states pertaining to the same doublet. For weakly hybridized states $|k_1\rangle$ and $|k_2\rangle$, provided that the value of tunnel splitting is much smaller than pulse detuning from one of these states, we can write $\delta_{k_1} \approx \delta_{k_2}$.

We suppose, that the pulse energy bandwidth is much larger than $|\delta_{k_1} - \delta_{k_2}|$ so we are unable to resolve the doublet states under consideration. Furthermore, in this case $\lambda_{0k_1} \approx \lambda_{0k_2}$, $\lambda_{0k_1} \approx \lambda_{1k_1}$, and $\lambda_{0k_2} \approx -\lambda_{1k_2}$ (see Sec. IV B). Therefore, the terms $\lambda_{0k}\lambda_{1k}/\delta_k$ arising from these states have opposite signs and cancel each other, so that the contribution of the doublet $\{|k_1\rangle, |k_2\rangle\}$ to Λ_2 is minimal. To estimate the contributions from higher states with energies $\varepsilon \geq -0.05$, we should take into account two circumstances. i) The ODT matrix elements between logical states and excited states with equal l decrease with the energy growth whereas the detunings increase with the energy growth. ii) High-lying states are closely spaced to each other and the distance between two neighboring states (not necessarily from same doublet) decrease rapidly with the energy growth. Thus, one may expect that corresponding terms in Λ_2 will either cancel out each other, as it was for degenerate states, or have insignificant effect on the sum convergence because of their subsequent reduction versus state energy. We think that both issues are important and their cooperative effect takes place, establishing our observation on the oscillation type of p_{tr} . Strictly speaking, for long times T , when $\Omega_R T \gg 1$, this is not true, because an internal structure of the sum p_{tr} , containing the oscillating terms of different but close frequencies, causes these oscillations to be averaged out and p_{tr} tends to its average value $\sim \max(p_{tr})/2$.

Utilizing similar arguments, we specify an algorithm of choice of the pulse frequency and amplitude in off-resonant driving regime. First of all, we determine

the doublet whose states $|\tilde{k}_1\rangle$ and $|\tilde{k}_2\rangle$ are characterized by sufficiently large ODT matrix elements and high tunneling rates (large value of the energy splitting in comparison with the pulse energy bandwidth). Then, by adjusting the pulse frequency to the center of energy gap between doublet states, we obtain for detunings $\delta_{\tilde{k}_1} = -\delta_{\tilde{k}_2}$. In this case, the terms $\lambda_{0k}\lambda_{1k}/\delta_k$ enter into Λ_2 with the same sign resulting in amplification in the sum. Doing so, we should remember that the field energy ε_{field} (i.e., pulse strength) must be much smaller than the doublet energy splitting. As it can be seen from Fig. 2 (b), upper bound value for ε_{field} is to be set ~ 0.005 at the whole considered range of R . Actually, it means that we can reliably operate with frequencies that fall within the interval containing the states from HMI subbands with $n = 3$ and $n = 4$. Moreover, the frequency choice just outlined cannot guarantee low population of excited states. A general way to minimize this population implies the use of moderate pulse strengths at fixed detunings. Note, that two-level Rabi oscillation regime with $\max(p_{tr}) < 0.01$ can be achieved under this frequency choice, since marked points on Fig. 7 lie in the middles of energy gapes separating the doublet states $|5g\sigma_g\rangle - |6h\sigma_u\rangle$, $|6g\sigma_g\rangle - |7h\sigma_u\rangle$, and $|7i\sigma_g\rangle - |8j\sigma_u\rangle$. With that, the pulses have to be strong enough in order to perform qubit rotations in the times that are shorter than decoherence time. For the off-resonant driving scheme, where the decoherence effects due to the finite population of excited states (e.g., the electron-phonon relaxation) are reduced considerably, the dephasing of localized states is expected to be the main source of coherence losses. In our

simulations we require that the operation times ($T_{op} \sim 1/\Omega_R$) do not exceed 10^{-8} s. It gives a lower bound value on the pulse strength to be $\varepsilon_{field} \sim 0.001$. For Si:P₂⁺ structure parameters, the allowed range $0.001 < \varepsilon_{field} < 0.005$ corresponds to the pulse strengths of hundreds of V/cm that is by two orders smaller than the field strengths considered in the voltage-based driving schemes [12] - [16].

Provided that the pulse parameters are selected correctly, the probability amplitudes c_0 and c_1 (and, consequently, probabilities p_0 and p_1) evolve smoothly against time thus allowing one to continuously rotate qubit state vector along fixed meridian with $\varphi = \pi/2$ on the Bloch sphere, namely, to create the superposition of logical states of the form $|\Psi(t)\rangle = \sqrt{p_0(t)}|0\rangle - i\sqrt{p_1(t)}|1\rangle$, where $p_0(t) + p_1(t) \approx 1$. Control over relative phase between logical states, needed for creation of an arbitrary superposition state of the qubit, requires the logical states to be addressed independently by two different pulses to maintain $\Lambda_0 \neq \Lambda_1$ in Eq. (20). To achieve this goal, one should break the central symmetry of HMI making use of external field, thus the important quantum operations given by Eqs. (34) - (36) will be realized in this case after application of bichromatic pulse. Besides, there exists a more familiar way utilizing the adiabatically varied bias field to produce a shift between the energies of logical states.

D. Phase and population dynamics in nonzero-bias case

As it was demonstrated in the works [3], [16], [20], and [30], an uniform electrostatic field, polarized along z axis, disturbs spatial symmetry of DD structure

relative to the origin and produces a necessary energy shifts. The Hamiltonian of HMI, subjected to the action of an external axial field, reads $H = H_0 - eE_0z$. We compute the eigenfunctions $\{|\tilde{\Psi}_i\rangle\}$ of HMI with the field, expanding them over the eigenfunctions $\{|\Psi_k\rangle\}$ without the field: $|\tilde{\Psi}_i\rangle = \sum_k \tilde{C}_{ki} |\Psi_k\rangle$. The eigenenergies and the expansion coefficients \tilde{C}_{ki} are calculated directly through the diagonalization of the Hamiltonian in the basis of 64 σ -states, found in Sec. IV A. Similarly, the ODT matrix elements $\{\tilde{d}_{ij}\}$ between the HMI eigenstates in the non-zero bias case are expressed via the ODT matrix elements between the HMI eigenstates in the zero bias case, $\{d_{mn}\}$, as follows: $\tilde{d}_{ij} = \sum_{m,n} \tilde{C}_{mi}^* \tilde{C}_{nj} d_{mn}$.

The dependencies of eigenenergies on static field energy ε_{field}^{st} (defined in complete analogy with ε_{field}) are given at Fig. 8 for internuclear distance $R = 38$. With respect to the hybridization degree of HMI states at $\varepsilon_{field}^{st} = 0$, the important difference in energy behavior of states, originated from localized and delocalized states, is observed at $\varepsilon_{field}^{st} \neq 0$. We see that the energies of states, corresponding to weakly hybridized states of HMI without bias field (e.g., the states from subbands with $n = 1$ and $n = 2$), are approximately linear functions of ε_{field}^{st} (due to Stark effect). The generation of the energy difference $\Delta = \varepsilon_1 - \varepsilon_0 = \varepsilon_{field}^{st} R$, where $R = 38$, requires an application of bias field with the strength $E_0 \sim 10$ V/cm (see Fig. 8 (a)). If $\varepsilon_{field}^{st} > 0$, the states, whose energies bring down (up) with the static field strength, are localized predominantly on "deep" donor B ("shallow" donor A). From Fig. 8 (b) one can observe a general tendency of the HMI spec-

trum to become complicated with the field growth due to both the full lifting of Coulomb degeneracy (in contrast to the partial lifting in HMI spectrum without field) and the hybridization of states pertaining to different subbands (giving rise to crossing-anticrossing pattern on Fig. 8 (b)). Otherwise, the energies of delocalized states $|5g\sigma\rangle$ and $|6h\sigma\rangle$ (thick red curves on Fig. 8(b)) vary with static field energy as $\varepsilon[5g(6h)\sigma] \approx \frac{1}{2}[\varepsilon(5g\sigma_g) + \varepsilon(6h\sigma_u)] \mp \frac{1}{2}\sqrt{(\varepsilon_{field}^{st}R)^2 + \Delta_{5g\sigma_g-6h\sigma_u}^2}$, where $\Delta_{5g\sigma_g-6h\sigma_u} = \varepsilon(6h\sigma_u) - \varepsilon(5g\sigma_g)$ is the tunnel splitting at zero bias field. It means that the tunneling rate for those states remains sufficiently high if $|\varepsilon_{field}^{st}| \leq 0.001$. Therefore, we shall continue to operate with those states exploiting them as the transport channels. The dependencies of the matrix elements on the field strength for transitions, connecting logical states and transport states $|5g\sigma\rangle$ and $|6h\sigma\rangle$, are given on Fig. 9. The examination of the values of matrix elements confirms the fact that the maximum of electron density for the state $|5g\sigma\rangle$, originated from symmetric state $|5g\sigma_g\rangle$, is displaced onto "deep" donor B , whereas for the state $|6h\sigma\rangle$, originated from asymmetric state $|6h\sigma_u\rangle$, it goes onto "shallow" donor A . The deeps on the curves appear due to the electron density redistribution at crossing/anticrossing points, where transport states interact with localized states (see Fig. 8 (b)).

In Ref. [17], it was demonstrated that elementary single-qubit operations can be performed in asymmetric DD structure, driven by two resonant pulses. Here we check this proposal for zero-detuning case by the simulation of NOT operation. According to our previous results, the resonant asymmetric three-level scheme requires

that $|\lambda_{0tr}| = |\lambda_{1tr}|$, or $|E_0/E_1| = |d_{1tr}/d_{0tr}|$. Since the ODT matrix elements for distinct arms of the excitation scheme differ from each other, we need to compensate the difference in coupling coefficients λ_{0tr} and λ_{1tr} by choosing the pulse strengths so that to fulfill above condition. Now we integrate Eq. (6) with the right-hand side defined by the set $\{\tilde{d}_{ij}\}$ of the ODT matrix elements and with the initial conditions reflecting the localization of electron at the beginning of pulse action in the ground state $|0\rangle$. As usual, the probabilities $p_0(T)$, $p_1(T)$, and $p_{tr}(T)$ (Fig. 10) illustrate the qubit state inversion for the case when both pulses are in the exact resonance with the state $|5g\sigma\rangle$ (the other parameters are indicated at the plot). We can reveal that the arms of excitation scheme remain inequivalent, despite of that the couplings have been balanced. The time dependency of p_1 is smooth, but the plot for p_0 demonstrates a fringes superimposed on ideal "three-level" curve (compare with that pictured on Fig. 5) and originated from non-resonant excitation of "deep" donor states whose energies lie closely to the $|5g\sigma\rangle$ states. For $\varepsilon_{field}^{st}=0.0004$, the difference between energy of transport state and those of the states of donor B is ~ 0.006 , whereas the energies of states localized on donor A lie by ~ 0.02 higher than the transport state energy. Add, that the character of dynamical picture is not changed noticeably, if one uses the state $|6h\sigma\rangle$. To suppress these fringes and refine oscillation picture, one should apply the pulses with lower strengths. In spite of presence of these perturbations, the electronic transfer probability is very high and the period of the oscillations is short enough. We expect this type of evolution to be

conserved for various quantum operations carried out in asymmetric DD structure under the resonant excitation regime.

Unlike in the case of symmetric HMI, here we were unable to find pulse parameters for asymmetric off-resonant driving scheme that would provide a robust and fast implementation of basic quantum operations. This lack takes place because the pulse with frequency ω_0 , being tuned slightly below the state $|5g\sigma\rangle$ for the transition $|0\rangle \leftrightarrow |5g\sigma\rangle$, addresses unwanted nearly-resonant transitions connecting the state $|1\rangle$ with the states localized on "shallow" donor. Thus, the selectivity requirement is violated. The attempts to achieve the reliable two-level oscillation picture have forced us both to reduce the pulse strengths and to vary the detuning in such a way that both pulses would drive only the transitions prescribed by ideal excitation scheme. The goal is likely to be attained by this method, but the characteristic times will be inappropriately long in comparison with decoherence time. In particular, the asymmetric off-resonant scheme, described in Sec. III, will function correctly if Δ is much smaller than the energy spacings between the states lying around the energy $\varepsilon_0 + \omega_0$. At same time, the coupling coefficients must be much smaller than Δ , in order to address separately each arm of driving scheme by its own pulse. From the Fig. 8 (b) we obtain the estimations $\varepsilon_{field}^{st} < 10^{-4}$ and $\Delta < 0.004$ that, in its turn, implies $|\lambda_{0(1)k}|$ to be less than 10^{-3} . It tells us that under these conditions the off-resonant Rabi frequency Ω_R is of order of 10^8 s^{-1} (or smaller) that is out of interest of this paper.

Actually, it means that we can only deal with symmetric DD structure where the possibility of realization of the off-resonant qubit-state σ_X rotation has been already demonstrated. However, we know this type of quantum evolution is not sufficient for implementation of arbitrary quantum operation, since the phase control is also required. This difficulty may be overcome with the help of direct introduction of the phase difference between logical states by the voltage pulse that produces necessary energy shift. This technique is widely used in quantum dot structures to align the energy levels of different dots that is needed for experimental investigations of their transport and spectral properties. Here we consider a simplified model of voltage pulse action on the HMI replacing non-isotropic electric field, generated by the gate V_a (Fig. 1 (a)), by uniform axial electric field, as it is demonstrated at Fig. 1 (b). The time dependency of voltage pulse is approximated by the step function. In this case, elementary calculations predict the qubit phase oscillations with the frequency $\Omega_{phase} = \Delta/\hbar$. The general expression for qubit-state evolution operator in the two-level approximation, accounting for different voltage pulse shapes, can be found in Ref. [30]. We illustrate this type of quantum dynamics at Fig. 11, where two-level Rabi oscillations between the states $|+\rangle_H = (|0\rangle + |1\rangle)/\sqrt{2}$ and $|-\rangle_H = (|0\rangle - |1\rangle)/\sqrt{2}$ obtained from logical states by the Hadamard rotation, are presented. Relative to computational basis, these oscillations indicate on the phase dynamics generated by the operator σ_Z . For example, the application of voltage pulse during one-half oscillation period amounts to the phase shift by π between the

states $|0\rangle$ and $|1\rangle$ and takes about several picoseconds. With that, the population leakage from logical subspace remains negligible ($p_{tr} < 10^{-6}$). At the intersection points, the Hadamard superpositions $|\pm\rangle_H$ collapse into one of logical states.

Summarizing the results obtained in this and previous subsections, we conclude the numerical study of electron dynamics by observation that the strategy, utilizing sequential implementation of σ_X and σ_Z rotations, appears to be more reliable than the strategy based on simultaneous action of voltage and optical pulses. With that, one may regard the formulas deduced in Sec. III for asymmetric off-resonant scheme as describing non-ideal nearly-symmetric scheme driven by single pulse, where other external fields (e.g., acting on nearest qubits) slightly disturb the spatial symmetry of structure in uncontrollable way. In this case, small differences in frequencies of the arms quantified by the asymmetry parameter Δ , will amount to quantum error.

Of course, we should take into account that the driving scheme of Eqs. (34) - (36), whose efficiency has not been confirmed above for effective HMI, can describe the qubit dynamics for other models of DD structure (for example, that of heteropolar molecular ions [16]). The main issue, that makes the verification of proposed algorithm of quantum control difficult, is concerned with necessity to know in details the energy spectrum and the ODT matrix elements for each structure under consideration.

V. DISCUSSION

To provide more clarity in the understanding of the advantages of the charge qubit-

state engineering presented above, let us compare the resonant and off-resonant excitation schemes. The resonant optical driving of the DD structure modelled by single three-level scheme has been studied in Refs. [17, 18]. In the case considered here a more complex dynamics can take place involving more than one three-level scheme. For example, if we tune the lasers on resonance with the transition between the logical subspace $\{|0\rangle, |1\rangle\}$ and a state $|r\rangle$, $r \in \{k\}_{exc}$ located near the top of the barrier, a number of states with the energies close to ε_r will be excited as well. This picture is quite expected in the hydrogen-like molecular ions for the high-lying states which energies are within the interval $\Delta\varepsilon_r \leq |\lambda_{0(1)r}|$. However, for the symmetric structure it means that there will be no transitions between the qubit states. It is because the excited states belonging to the same doublet are presented by the symmetric and antisymmetric superpositions of the excited states of isolated donors which, being excited simultaneously, interfere constructively on one donor and destructively on another one. As a consequence, the donors are excited independently. This effect becomes more significant as the interdonor distance R increases and the tunnel coupling between the donors decreases. We have observed such type of electronic dynamics when pulse was tuned into resonance with low-lying excited states with $l = s, p, d, f$. When the energy splitting of the maximally-resolved doublet becomes comparable with the coupling coefficients of the optical dipole transitions, the process of the electron transfer between the donors is terminated. Note that the optically driven DD structure will demonstrate the similar behavior if one of

the pulses is short enough so that its duration is $T \leq 1/\Delta\varepsilon_r$ and thus it contains harmonics in the frequency range $\delta\omega \sim 1/T \geq \Delta\varepsilon_r$. Again, the states with the energies belonging to the interval $\Delta\varepsilon_r$ will be excited simultaneously giving rise to the electron transfer blockage just outlined. In our simulations, we have arrived at this regime via application to HMI a short and intense ($\varepsilon_{field} \sim 0.1$) pulse.

The reliable resonant scheme thus deals with single transport state (for HMI, the states $|5g\sigma_{(g)}\rangle$ and $|6h\sigma_{(u)}\rangle$) and is very sensitive to the pulse detuning from the resonance with that state. For example, the non-zero detuning always produces an amplitude error in NOT gate because of incomplete depopulation of the initial state when the pulse is off [21]. On the contrary, the use of the off-resonant pulses enables one to exploit the whole number of excited states (from which only several ones participate substantially in electronic dynamics). Moreover, we don't need to control the pulse frequencies with high accuracy since a small variation in the pulse detunings brings about an insignificant change in the Rabi frequency (see Fig. 7). The computational errors originated from the frequency renormalization can be corrected by the corresponding change in the pulse duration due to the smooth time dependencies of the probability amplitudes, as it was shown at Fig. 6. The only requirement that must be followed closely for successful electron state manipulations is the Raman two-photon resonant condition (9).

The selectivity of the electron resonant transfer requires also a strict control over the pulse polarizations. The transport states in the molecular ion are formed through

the hybridization of those individual donor states whose wave functions are extended along the axis z that coincides with the interdonor direction. Other states (e.g., π -states) are hybridized weakly and cannot assist efficiently in the electron dynamics. Their excitations are due to the pulse components polarized along the axes x and y . It amounts to the population leakage into the non-hybridized single-donor states with the energies lying in the close proximity to the energy of the transport state. Let us define the small angles γ_{nx} and γ_{ny} that characterize the deviations of the n -th pulse polarization from the axis z :

$$\mathbf{E}_n = \mathbf{E}_{nz} + \mathbf{E}_{nx} \cos(\pi/2 + \gamma_{nx}) + \mathbf{E}_{ny} \cos(\pi/2 + \gamma_{ny}), \quad (42)$$

$$|\gamma_{nx}|, |\gamma_{ny}| \ll 1, \quad n = 0, 1,$$

then the probability of successful implementation of the quantum operations is reduced by a factor of $w \sim 1 - \max(\gamma_{nx}^2, \gamma_{ny}^2)$. In the off-resonant case, the populations of those states remain negligibly small ($\sim |\lambda_{nk}|^2 / \delta_k^2$) and the corresponding channel of population leakage is blocked.

The important difference between the resonant and off-resonant schemes lies in the treatment of the decoherence problem. We know the relaxation rates from the transport state caused by the spontaneous photon/phonon emission during the resonant excitation [18] may be high enough to corrupt the qubit state. In the off-resonant scheme the population of the intermediate state(s) is negligible and the probability of relaxation is drastically reduced. The influence of the residual population of the intermediate state on the adiabatic electron transfer in the three-level scheme was examined in Ref. [31] for the gaussian pulses. It was shown that

the error introduced by the spontaneous emission together with the error due to the non-adiabaticity are inversely proportional to the pulse detuning and can be made small enough to allow the fault tolerant quantum computation.

Note that the complete population transfer between the qubit states, or NOT operation, requires that $\Lambda_0 = \Lambda_1$. This is naturally met for nearly symmetric DD structures where $\Delta \approx 0$ and $|\mathbf{d}_{0k}| \approx |\mathbf{d}_{1k}|$. In general, however, one should keep in mind that $|\mathbf{d}_{0k}| \neq |\mathbf{d}_{1k}|$ that makes the performing of the condition $\Lambda_0 = \Lambda_1$ very problematic. It seems then reasonable to point the other way for the population transfer based upon the pulse-shaped techniques. Such methods, e.g., the stimulated Raman adiabatic passage (STIRAP) [26], are very robust against the pulse/structure imperfections and would allow one to handle the quantum information carefully. The theory of the adiabatic population transfer via multiple intermediate states, including the off-resonant case, was presented in Ref. [27]. Note that for the pulses strongly detuned from the resonance, the time ordering is no more important since successful population transfer may be attained for both intuitive and counterintuitive pulse sequences. If initially $c_0(t_0) = 1$, $c_1(t_0) = 0$, the intuitive (counterintuitive) pulse ordering means that $\lim_{t \rightarrow t_0} [f_0(t)/f_1(t)] = \infty(0)$ and $\lim_{t \rightarrow T} [f_0(t)/f_1(t)] = 0(\infty)$ and, as it follows from Eq. (24), $\Theta(t_0) = 0(\pi)$, $\Theta(T) = \pi(0)$. The population transfer may be understood as the adiabatic temporal development of the eigenstate $|+\rangle$ ($|-\rangle$) for the intuitive (counterintuitive) pulse ordering. As it is seen from Eq. (32), the qubit state inversion is realized in the asymmetric DD structures if the conditions

$\arg[\Lambda_2(T)] \pm \tilde{\Omega}(T) = \pi n$ and $T\Delta = \pi(2m+1)$ are fulfilled. The detailed analysis concerning the arrangement of the pulse shapes in STIRAP can be found elsewhere [26].

The effect of the detuning δ_{two-ph} from two-photon resonance (the spacing between dashed horizontal lines on Fig. 1 (b)) should be also taken into account at more profound level of investigations. In nearly-symmetric off-resonant case ($|\Lambda_0 - \Lambda_1| \ll |\Lambda_2|$) the problem enables analytical solution. If electron was initially localized into the state $|0\rangle$, the total excitation probability (including transfer probability into state $|1\rangle$) at large detunings ($|\Lambda_2| \ll |\delta_{two-ph}|$) is of order of $(\Lambda_2/\delta_{two-ph})^2 \ll 1$. Therefore, if the detunings from two-photon resonance are significant, electronic excitations from localized state $|0\rangle$ do not occur. In the opposite case of small detunings, i.e., when $|\delta_{two-ph}| \ll |\Lambda_2|$, the probability of successful electronic transfer is given by formula $p_1 \approx 1 - (\delta_{two-ph}/2\Lambda_2)^2$ (provided that other parameters are chosen in optimal way).

Finally, in our analytical treatment we consider continuum states only as virtually excited transport channels, neglecting the possibility of two-photon resonant electron transitions from logical subspace into the continuum states, that reside within interval around the energy $\varepsilon_{2\omega_0} = \varepsilon_0 + 2\omega_0$, via intermediate low-lying excited states (not necessarily highly populated) with energies $\sim \varepsilon_0 + \omega_0$. It is known that in isolated hydrogen atom the matrix elements for the transition $|1s\rangle \leftrightarrow |2p\sigma\rangle$ and the matrix elements for transitions connecting the state $|2p\sigma\rangle$ with s (or d) continuum

waves with energies pertaining to the interval pointed above, have the same order of magnitude. Hence, one could expect the electron dynamics in DD structure induced by optical driving pulses to be much more complex. However, in experimental investigations of low-frequency excitations in atomic systems these processes do not manifest themselves at the level that would establish the necessity to include the continuum into theoretical model. Perhaps, it could be explained by the arguments we have used in Sec. IV C to account for our numerical results reflecting very small influence of high-lying states of discrete part of HMI spectrum on electron dynamics. In principle, the continuum states being addressed directly can also be used as transport channels, but, at the same time, can bring about additional decoherence (see, e.g., [32]).

VI. CONCLUSIONS

In this paper we have considered the one-electron double-donor structure subjected to the action of optical and electrostatic pulses. Unlike the other systems proposed to serve as the potential candidates for the solid state optically-controlled qubits (double quantum dots, rf-SQUIDs), the double-donor structure is characterized by sufficiently high density of the bound states at the edge of the barrier that separates the donors. It means that the three-level resonant scheme proposed earlier to implement the desired qubit-state evolution may be unsuitable to maintain the appropriate selectivity of the optical excitations. On the other hand, the off-resonant scheme looks as more efficient for the qubit manipulations and robust in

comparison with the resonant scheme. Though the Raman evolution of the qubit is slower than that in the case of the resonant driving, it seems to be more reliable for the implementation of quantum operations. We have shown that the basic single-qubit operations may be performed on the DD structure for several pulse and structure parameter choices. Numerical simulations, carried out on structure modelled by effective hydrogen molecular ion, have confirmed the validity of our analytical framework where three important simplifications, concerning the treatment of dynamical problem, have been made. There are: i) rotating-wave approximation, ii) adiabatic elimination, and iii) neglecting the transitions between high-lying states. Although all of them are widely used, it is, to our knowledge, for the first time when these approximations are verified in rather complicated dynamical study of multilevel system.

The information about the structure and pulse parameters is contained in the Rabi frequency of the two-level oscillations. This frequency can be defined experimentally for each set of the detunings, the strengths, and the durations of the pulses. The results of those measurements could be used to reconstruct the features of the spectrum of the DD structure.

Note that the method of the electron-state manipulations by optical means can be applied also to the spin-based encoding schemes like that of Ref. [2]. The implementation of optically controlled effective electron spin exchange described in Ref. [33] for the two-electron double-dot structure, can be generalized on the two-

electron DD structure. The use of the adiabatic schemes is of the particular interest.

ACKNOWLEDGMENTS

Discussions with L. A. Openov are gratefully acknowledged.

References

- [1] S. R. Schofield, N. J. Curson, M. Y. Simmons et al., Phys. Rev. Lett. **91**, 136104 (2003); F. J. Rueß, L. Oberbeck, M. Y. Simmons et al., Nanolett. **4**, 1969 (2004); D. N. Jamieson, C. Yang, T. Hopf et al., Appl. Phys. Lett. **86**, 202101 (2005); T. Shinada, S. Okamoto, T. Kobayashi, and I. Ohdomari, Nature **437**, 1128 (2005).
- [2] B. E. Kane, Nature **393**, 133 (1998).
- [3] L. C. L. Hollenberg, A. S. Dzurak, C. Wellard et al., Phys. Rev. B **69**, 113301 (2004).
- [4] X. Hu, B. Koiller, and S. Das Sarma, Phys. Rev. B **71**, 235332 (2005).
- [5] R. Vrijen, E. Yablonovitch, K. Wang et al., Phys. Rev. A **62**, 012306 (2000).
- [6] A. J. Skinner, M. E. Davenport, and B. E. Kane, Phys. Rev. Lett. **90**, 087901 (2003).
- [7] M. Friesen, C. Tahan, R. Joynt, and M. A. Eriksson, Phys. Rev. Lett. **92**, 037901 (2003).
- [8] A. D. Greentree, A. R. Hamilton, L. C. L. Hollenberg, and R. G. Clark, Phys. Rev. B **71**, 113310 (2005).

- [9] Kai-Mei C. Fu, T. D. Ladd, C. Santori, and Y. Yamamoto, Phys. Rev. B **69**, 125306 (2004).
- [10] L. C. L. Hollenberg, C. Wellard, C. I. Pakes, and A. G. Fowler, Phys. Rev. B **69**, 233301 (2004).
- [11] M. J. Testolin, A. D. Greentree, C. J. Wellard, and L. C. L. Hollenberg, Phys. Rev. B **72**, 195325 (2005).
- [12] A. D. Greentree, J. H. Cole, A. R. Hamilton, and L. C. L. Hollenberg, Phys. Rev. B **70**, 235317 (2004).
- [13] L. C. L. Hollenberg, A. D. Greentree, A. G. Fowler, and C. J. Wellard, Phys. Rev. B **74**, 045311 (2006).
- [14] A. D. Greentree, S. J. Devitt, and L. C. L. Hollenberg, Phys. Rev. A **73**, 032319 (2006).
- [15] A. S. Martins, R. B. Capaz, and B. Koiller, Phys. Rev. B **69**, 085320 (2004).
- [16] B. Koiller, X. Hu, and S. Das Sarma, Phys. Rev. B **73**, 045319 (2006).
- [17] L. A. Openov and A. V. Tsukanov, Pis'ma Zh. Eksp. Teor. Fiz. **80**, 572 (2004) [JETP Lett. **80**, 503 (2004)].
- [18] L. A. Openov, Phys. Rev. B **70**, 233313 (2004); Zh. Eksp. Teor. Fiz. **127**, 973 (2005) [JETP **100**, 857 (2005)].

- [19] R. Köhler, A. Tredicucci, F. Beltram et al., *Nature* **417**,156 (2002); B. S. Williams, S. Kumar, and Q. Hu, *Opt. Express* **13**, 3331 (2005).
- [20] S. Barrett and G. J. Milburn, *Phys. Rev. B* **68**, 155307 (2003).
- [21] A. V. Tsukanov and L. A. Openov, *Fiz. Tekh. Poluprovodn. (S. Peterburg)* **38**, 94 (2004) [*Semiconductors* **38**, 91 (2004)].
- [22] E. Paspalakis, Z. Kis, E. Voutsinas, and A. F. Terzis, *Phys. Rev. B* **69**, 155316 (2004).
- [23] A. V. Tsukanov, *Phys. Rev. B* **73**, 085308 (2006).
- [24] S. Flügge, *Practical Quantum Mechanics II* (Springer - Verlag, Berlin - Heidelberg - New York, 1971).
- [25] L. Allen and S. R. Stroud Jr., *Phys. Rep.* **91**, 1 (1982).
- [26] N. V. Vitanov and S. Stenholm, *Opt. Commun.* **135**, 394 (1997).
- [27] N. V. Vitanov and S. Stenholm, *Phys. Rev. A* **60**, 3820 (1999).
- [28] G. D. J. Smit, S. Rogge, J. Caro, and T. M. Klapwijk, *Phys. Rev. B* **68**, 193302 (2003).
- [29] P. E. Falloon, *Theory and Computation of Spheroidal Harmonics with General Arguments*. Masters thesis. Chapter 9. Perth, Australia: Uni-

versity of Western Australia, 2001. (This material is available at <http://www.physics.uwa.edu.au/pub/Theses/2002/Falloon/MastersThesis.pdf>.)

- [30] A. V. Tsukanov and K. A. Valiev, *Mikroelektronika* **36**, 83 (2007) [Russian Microelectronics **36**, 67 (2007)].
- [31] X. Caillet and C. Simon, E-print archives, quant-ph/0510014.
- [32] A. M. Basharov and S. A. Dubovis, *Opt. Spektrosk.* **99**, 802 (2005) [*Opt. Spectrosc.* (Russia) **99**, 770 (2005)].
- [33] A. V. Tsukanov, *Phys. Rev. A* **72**, 022344 (2005).

FIGURE CAPTIONS

Fig. 1 (color online). a) Schematics of the quantum state manipulation in the one-electron double-donor structure. A pair of (phosphorous) donors A and B (one of them being singly-ionized) implanted into semiconductor (Si) matrix is addressed by optical pulse(s). Additionally, electrostatic pulse generated by voltage gate V_a varies the structural potential. The desired final orbital state of electron is attained due to cooperative effect of both pulses on the structure. b) Potential profile of DD structure, modelled by effective hydrogen molecular ion (see Sec. IV), along structural axis z . The qubit states $|0\rangle$ and $|1\rangle$ are defined by the localized orbital states of the donors A and B with the energies ε_0 and ε_1 , respectively. They are coupled to a collection of excited states by two optical pulses with the frequencies ω_0 and ω_1 . Uniform axial electrostatic field is applied across the structure in order to break the symmetry and to introduce the energy difference $\Delta = \varepsilon_1 - \varepsilon_0$. Here, the distance R between donor centers is 38 a.u. and the electrostatic field energy $\varepsilon_{field}^{st} = 4 \times 10^{-4}$ a.u. so that $\Delta = R \times \varepsilon_{field}^{st} = 0.0152$ a.u. The energies of the whole molecular ion are obtained from electronic eigenenergies + energy of internuclear repulsion $1/R$.

Fig. 2 (color online). The dependencies of electronic eigenenergies of 20 low-lying eigenstates from σ -subspace ($m = 0$) of hydrogen molecular ion on the internuclear distance R . a) Ground-state energies $\varepsilon(1s\sigma_g)$ and $\varepsilon(2p\sigma_u)$. b) Excited-state energies. Here, the eigenenergies of transport states $|5g\sigma_g\rangle$ and $|6h\sigma_u\rangle$ are presented by

thick red curves whereas the eigenenergies of the states which may also be used as transport ones are drawn by thick blue lines. The vertical dotted lines correspond to the internuclear separations $R = 22$ a.u., $R = 30$ a.u., and $R = 38$ a.u., for which dynamical simulations are performed.

Fig. 3 (color online). Characteristic electronic tunneling time $\tau_{1s\sigma_g-2p\sigma_u}$ between the localized states $|1s\sigma_g\rangle$ and $|2p\sigma_u\rangle$ of hydrogen molecular ion, calculated for parameters that correspond to single-valley approximation for Si:P₂⁺ double-donor structure, as function of the internuclear distance R .

Fig. 4 (color online). The values of matrix elements of optical dipole transitions, connecting the logical state $|0\rangle$ and the low-lying excited states pertaining to the hydrogen molecular ion subbands with a) $n = 2$, b) $n = 3$, and c) $n = 4$, as functions of the internuclear distance R .

Fig. 5 (color online). An example illustrating the resonant qubit-state manipulation. The time dependencies of probabilities $p_0(T)$ and $p_1(T)$ to find electron into logical states $|0\rangle$ and $|1\rangle$ and that of total probability $p_{tr}(T)$ to find electron into excited states are plotted for initial condition $c_0(0) = 1$, $c_{k \neq 0}(0) = 0$. The numerical solutions are given by solid curves, and the analytical solutions, presented by equation (40) and supplied with primes at the insets, are visualized by dashed curves. The pulse is in exact resonance with transport state $|6h\sigma_u\rangle$. Other parameters are given at the plot.

Fig. 6 (color online). An example illustrating the off-resonant qubit-state manipu-

lation. The probabilities $p_0(T)$, $p_1(T)$, and $p_{tr}(T)$ demonstrate almost ideal two-level oscillation picture. The maximum of total probability of population leakage from computational subspace is 0.01. The pulse frequency is tuned into the middle of HMI subband with $n = 4$ (red-squared point on Fig. 7 (b)). Other parameters are given at the plot.

Fig. 7 (color online). The Rabi frequency $|\Lambda_2|$ for the off-resonant symmetric driving scheme is plotted vs the pulse frequency $\omega \equiv \omega_0$ at two values of pulse strength $\varepsilon_{field} = 0.003$ a.u. (blue). and $\varepsilon_{field} = 0.005$ a.u. (green) for internuclear distances a) $R = 30$ a.u. and b) $R = 38$ a.u. The curves correspond to analytical results of Eq. (21) whereas full circles mark the values of $|\Lambda_2|$ extracted from numerical data. Rabi frequencies, at which the probability p_{tr} of leakage from logical subspace is lower than 0.01, are enclosed into red open squares. Vertical dotted lines designate the energy levels near which off-resonant approximation becomes inapplicable.

Fig. 8 (color online). The electronic eigenenergies of HMI plotted in the dependence on static field energy ε_{field}^{st} for $R = 38$ a.u. Dotted vertical line designates the value $\varepsilon_{field}^{st} = 4 \times 10^{-4}$ a.u. for which the dynamical simulation is carried out. a) The energies ε_0 and ε_1 of logical states. b) The energies of excited states. Thick red curves denote the eigenenergies of doublet states $|5g\sigma\rangle$ and $|6h\sigma\rangle$ that remain delocalized in the presence of electrostatic field, and can be exploited as transport channels for resonant manipulations on electronic wave function.

Fig. 9 (color online). The matrix elements of optical dipole transitions, connecting

the logical states $|0\rangle$ (dashed curves) and $|1\rangle$ (solid curves) with the states $|5g\sigma\rangle$ and $|6h\sigma\rangle$, in the dependence on static field energy $\varepsilon_{field}^{st} > 0$ for $R = 38$ a.u.

Fig. 10 (color online). Resonant manipulation of electron orbital state in asymmetric HMI at the electrostatic field energy $\varepsilon_{field}^{st} = 4 \times 10^{-4}$ a.u. Both pulses are in exact two-photon resonance with state $|5g\sigma\rangle$ and their amplitudes (field energies $\varepsilon_{field\ 0}$ and $\varepsilon_{field\ 1}$) are chosen so as to equalize the coupling coefficients of effective three-level excitation scheme (see text for details).

Fig. 11 (color online). The populations $p_+(T)$ and $p_-(T)$ of Hadamard-rotated states $|+\rangle_H$ and $|-\rangle_H$ vs electrostatic pulse duration T . Two-state Rabi oscillations in the Hadamard frame illustrate dynamics of relative phase between logical states $|0\rangle$ and $|1\rangle$. The population leakage into excited states is negligible.

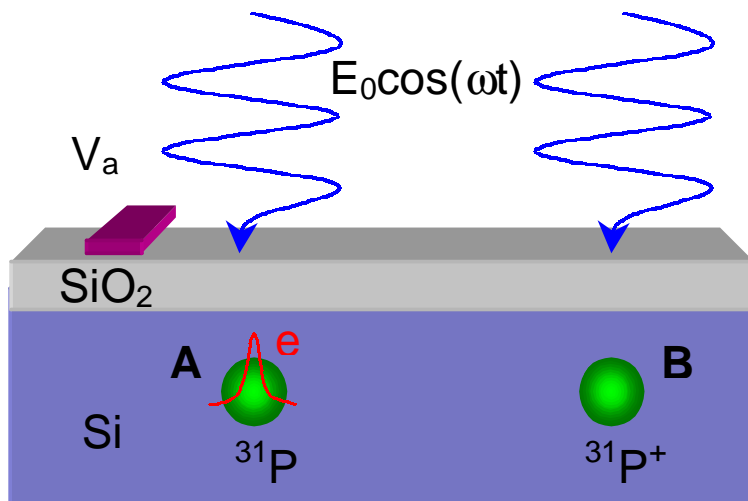


Fig. 1 (a)

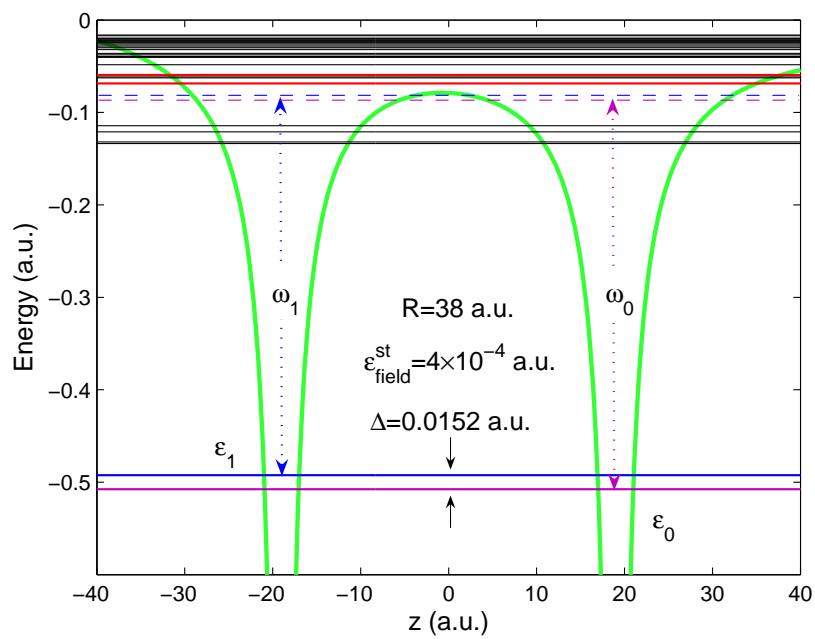


Fig. 1 (b)

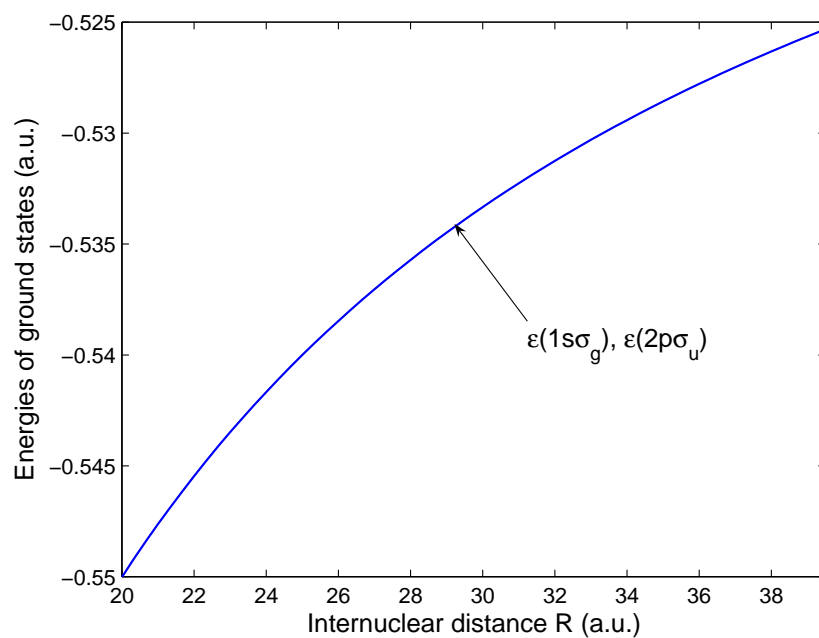


Fig. 2 (a)

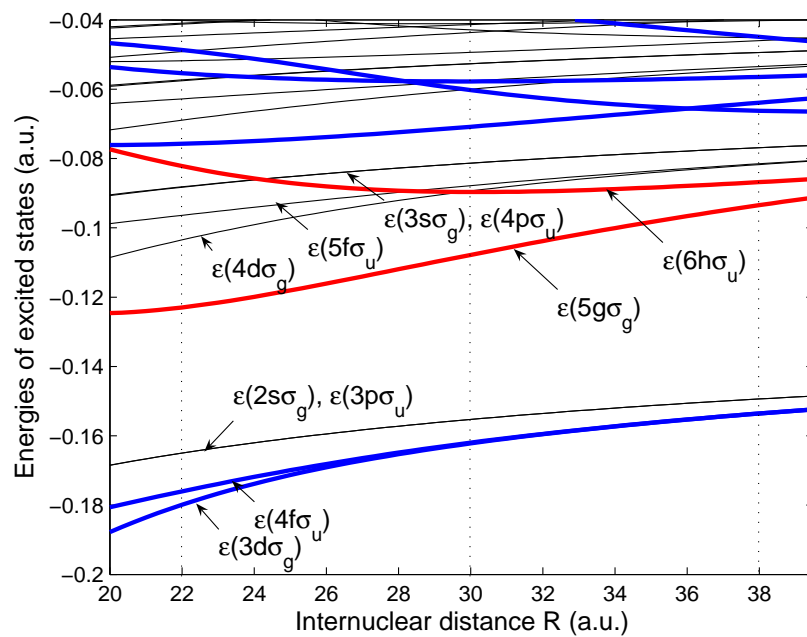


Fig. 2 (b)

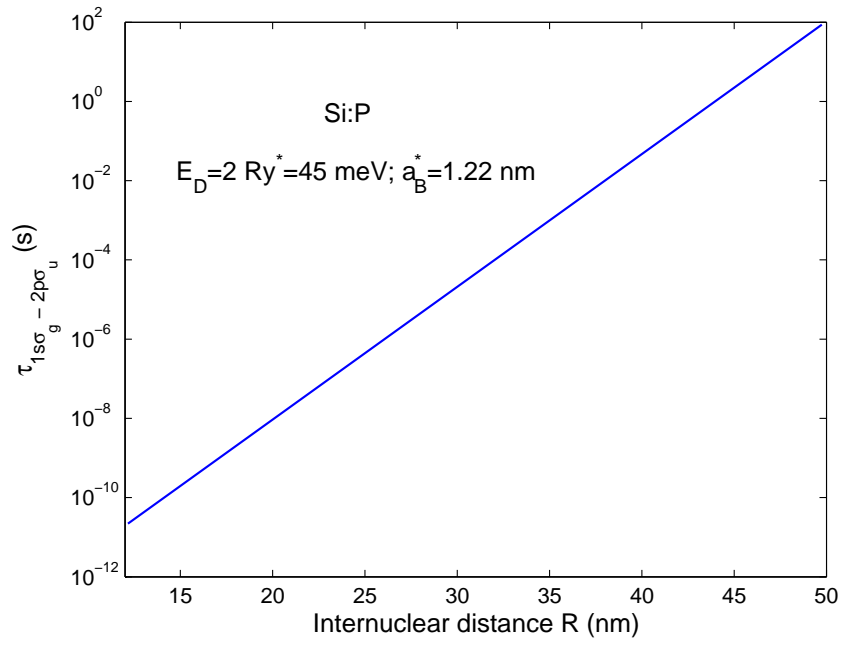


Fig. 3

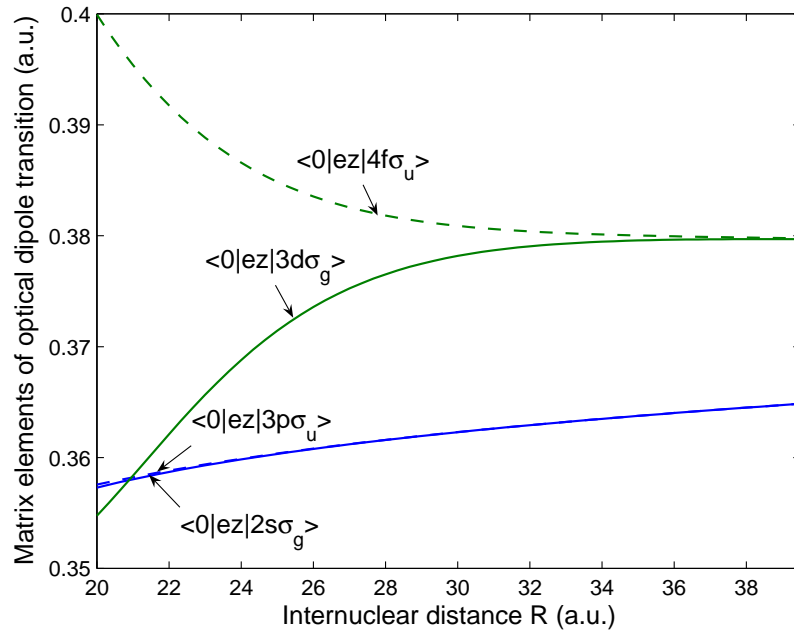


Fig. 4 (a)

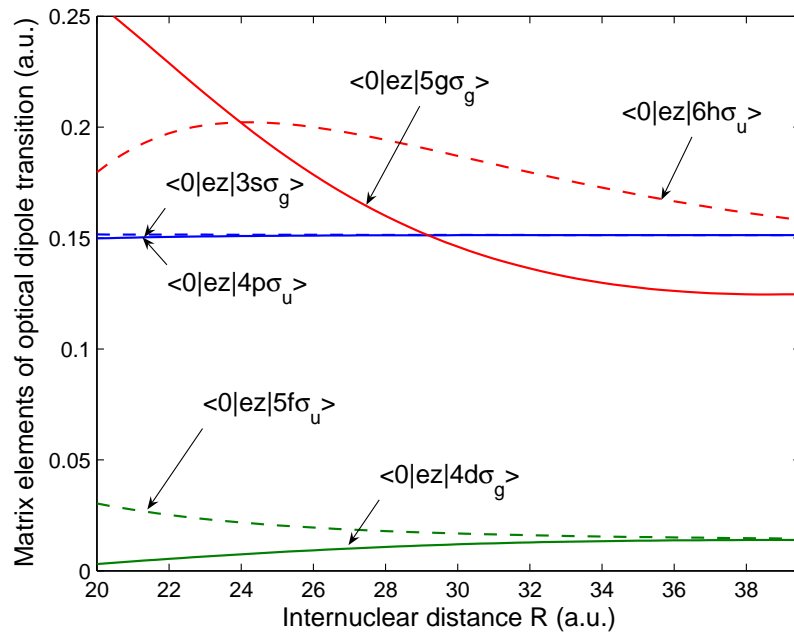


Fig. 4 (b)

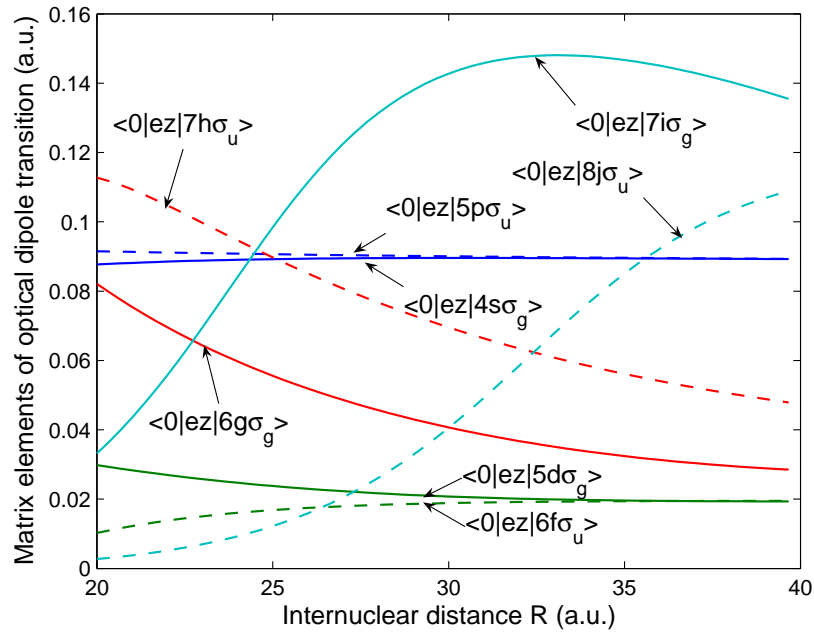


Fig. 4 (c)

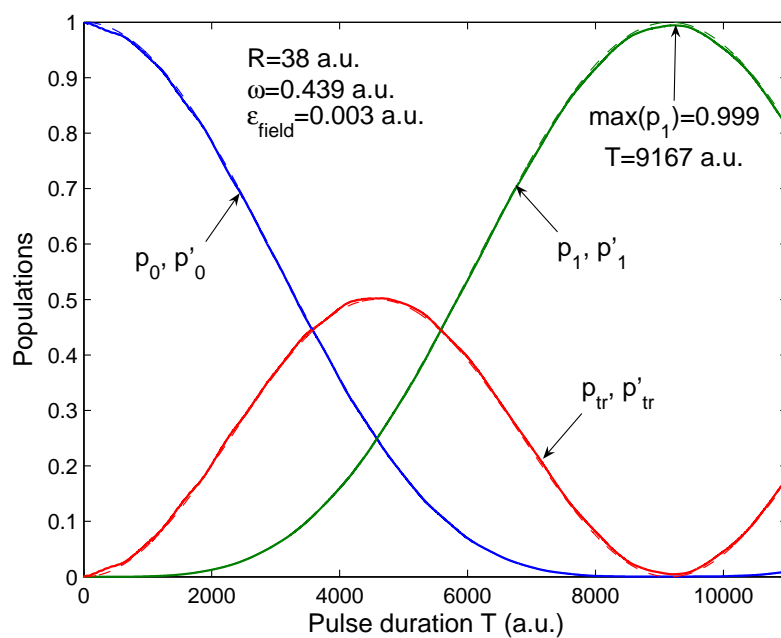


Fig. 5

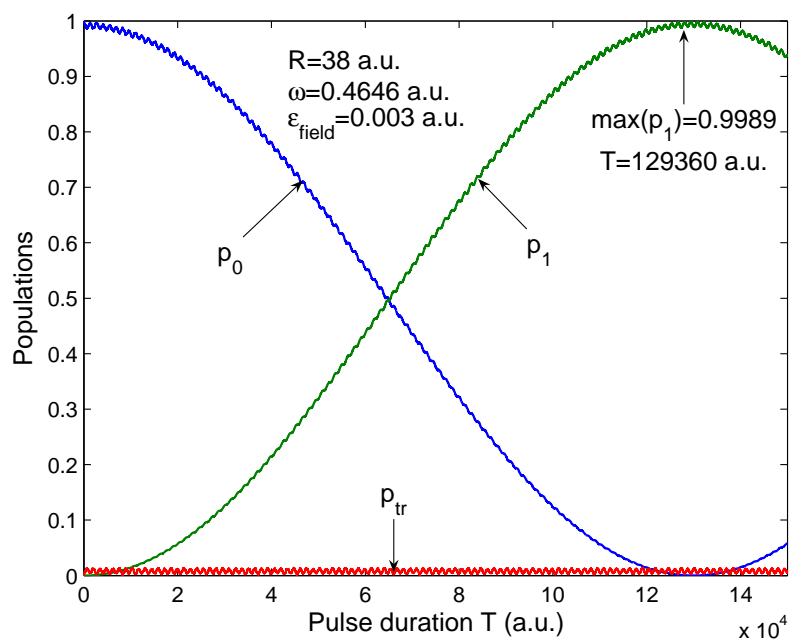


Fig. 6

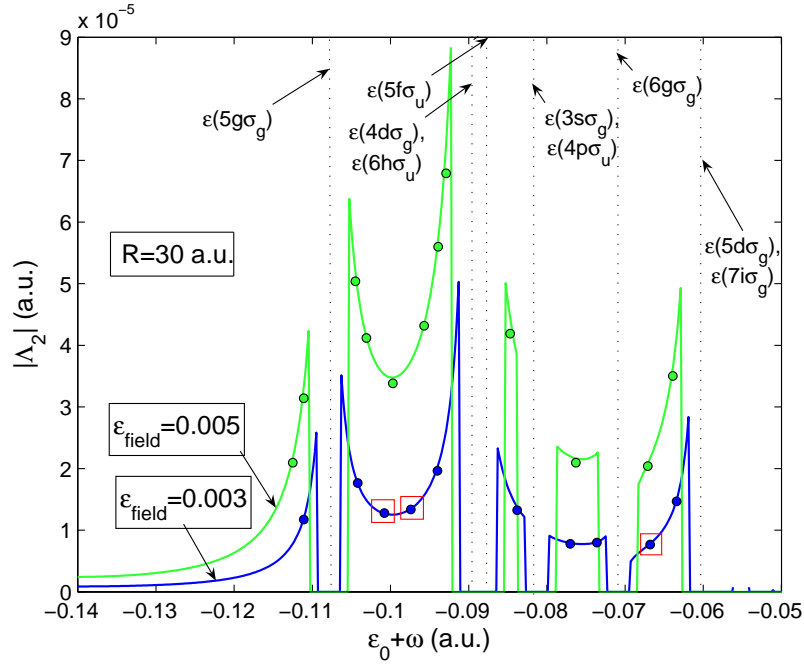


Fig. 7 (a)

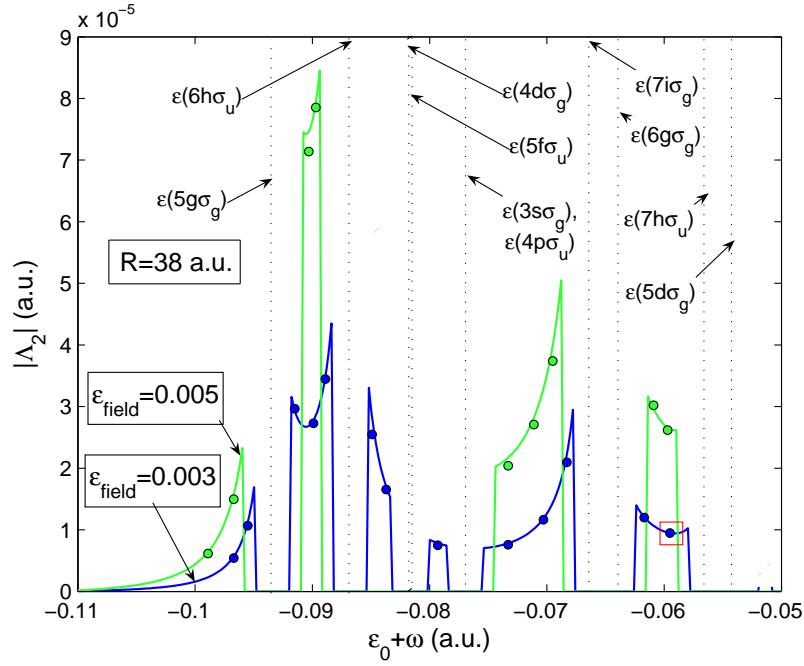


Fig. 7(b)

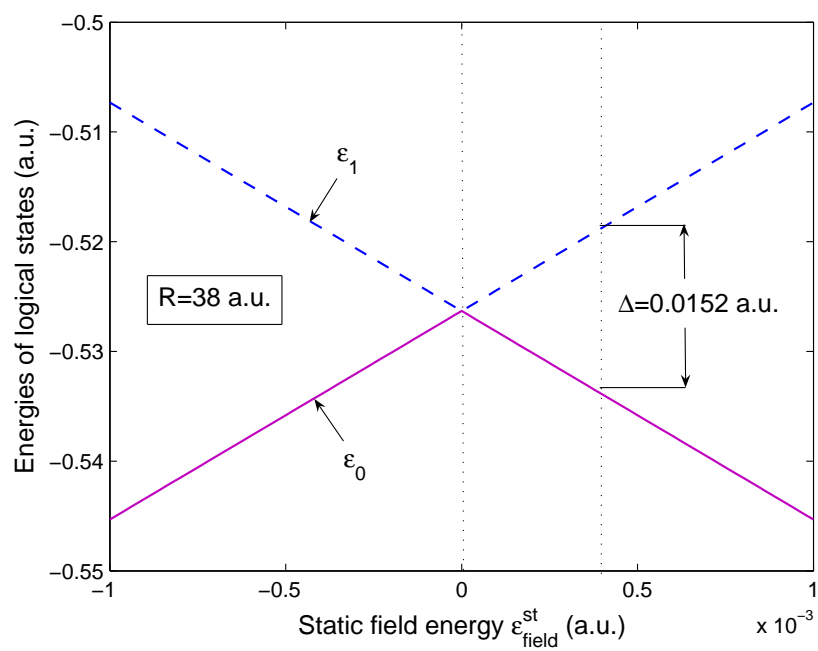


Fig. 8 (a)

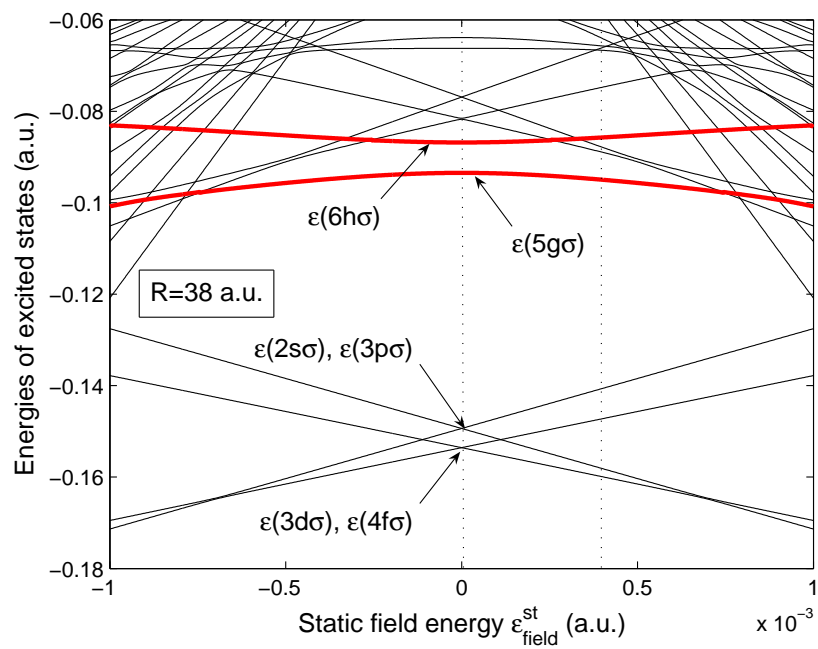


Fig. 8 (b)

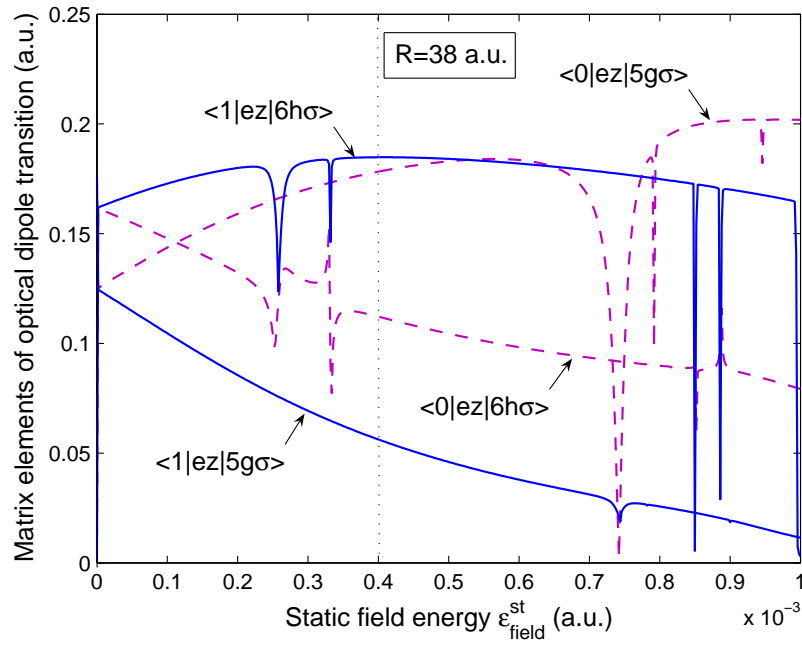


Fig. 9

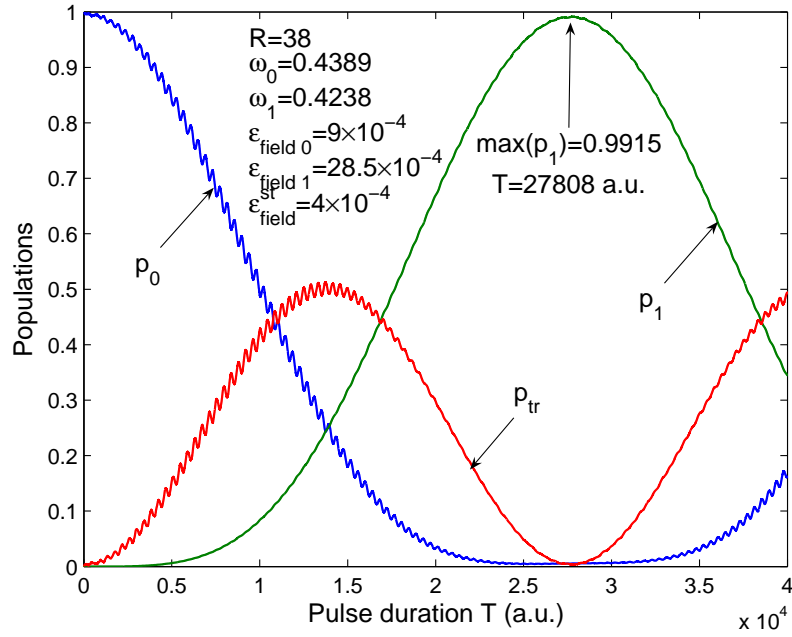


Fig. 10

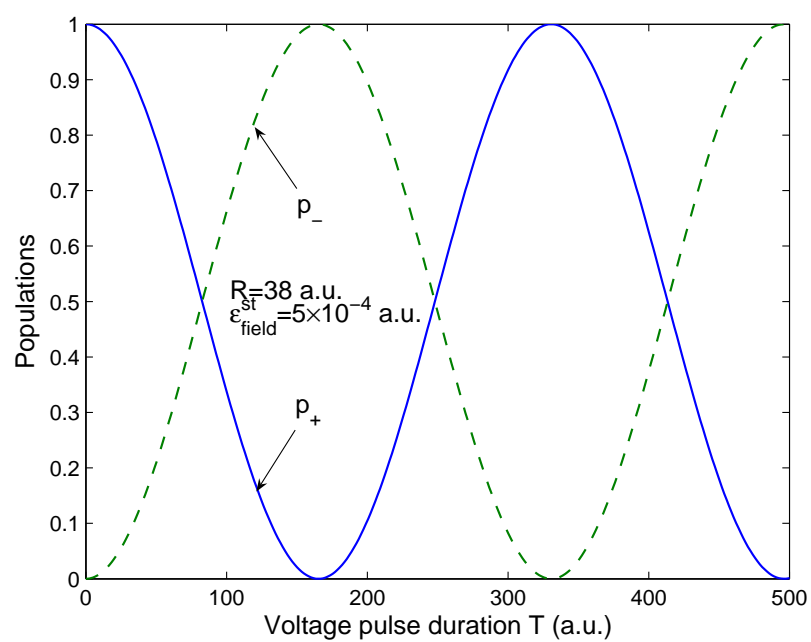


Fig. 11